Pan African University
Institute of Water and Energy Sciences

PAN-AFRICAN UNIVERSITY

INSTITUTE OF WATER AND ENERGY SCIENCES

(including CLIMATE CHANGE)

Master Dissertation

Submitted in partial fulfillment of the requirements for the Master degree in

Water Engineering

Presented by

Abdel Aziz O.R. GADO

Hydrological Modeling for Water Balance Components and Flood Hazard Assessment under Climate Change in Mono, Lower Basin, Benin and Togo

Defended on 04/09/2019 Before the Following Committee:

Chair	Ghenim Abderrahmane Ph.D	(University of Tlemcen, Algeria)
Supervisor	Navneet Kumar Ph.D	(ZEF, Bonn –Germany)
External Examiner	Tirusew Asefa Ph.D	(University of South Florida, USA)
Internal Examiner	Chabane Sari Sidi Mohamed Ph.D	(PAUWES, Algeria)

Academic Year 2018-2019

DECLARATION

I, Abdel Aziz O.R. GADO, the undersigned, declare that the thesis entitled *"*Hydrological Modeling for Water Balance Components and Flood Hazard Assessment under Climate Change in Mono, Lower Basin, Benin and Togo*",* is a result of my own work and that it has not been presented to any other learning institution for a similar award of degree, diploma or other professional. Where other sources of information have been used, they have been acknowledged. I understand that non-adherence to the principle of academic honesty and integrity, misrepresentation/fabrication of any idea/data/fact/source/ will constitute sufficient ground for disciplinary action by the university.

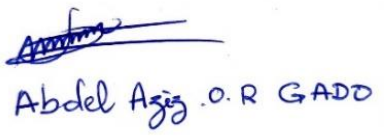

27.09.2019

Signature:

Abdel Aziz O.R. GADO Date

CERTIFICATION

This thesis has been submitted with my approval as the supervisor.

29.09.2019

Signature :

Dr.-Ing. Navneet KUMAR — Date

Center for Development Research (ZEF), University of Bonn, Germany

ACKNOWLEDGEMENT

Above all, I thank Almighty God for taking care of me throughout the duration of my studies.

I would like to send my sincere thanks to the African Union (AU) through Pan African University Institute of Water and Energy Sciences (PAUWES) including climate change for awarding me a scholarship to pursue my graduate studies in Algeria and also giving me a research grant to conduct my Masters' Thesis project.

My sincere appreciation goes to West African Science Centre on Climate Change and Adapted Land Use (WASCAL) including the scientific panel who spared no effort to support the accomplishment of this thesis.

I could also not complete this study without the support from numerous individual and organizations, therefore; I would like to express my heartfelt thanks to:

- My supervisor Navneet KUMAR, for his advice, guidance and motivation during the accomplishment of the present study. I am thankful to you.
- Dr. Jean HOUNKPE, who helped me during data collection and taught me engineering skills which were useful during the whole process of my thesis. I am deeply grateful for supporting and encouranging me.
- Dr. Aymar BOSSA, for welcoming me at WASCAL competence center and for guiding me during my stay.
- Dr.Yacouba Yira, for his thoughtful advice and his precious help.
- To my parents, friends and colleagues for their support.

LIST OF ABBREVIATIONS

AET: Actual Evapotranspiration

CORDEX: Coordinated Regional Climate Downscaling Experiment

DEM: Digital Elevation Model

DGEau : Direction Générale de l'Eau (Benin)

DMN : Direction de la Météorologie Nationale

EM-DAT : Emergency Events Data Base

EQM : Empirical Quantile Mapping

ETP: Evapotranspiration

GFDL-ESM2M: Global Coupled Climate – Carbon Earth System Models

HadGEM2-ES:Hadley Global Coupled Environment –Earth System Models

GCM: Global Climate Model

GDP: Gross Domestic Product

HBV-light: Hydrologiska Byråns Vattenbalansavdelning-light

IHMS: Integrated Hydrological Modelling System

IPCC: Intergovernmental Panel on Climate Change

NSE: Nash Sutcliff Efficiency

OK: Ordinary Kriging

RCM: Regional Climate Model

RCP: Representative Concentration Pathway

REMO: Regional Model

SDG: Sustainable Development Goal

SRES: Special Report on Emission Scenarios

SRTM: Shuttle Radar Topography Mission

UNDP: United Nations Development Program

UNFCCC: United Nations Framework Convention on Climate Change

USGS: United States Geological Survey

WMO: World Meteorological Organisation

TABLE OF CONTENTS

LIST OF FIGURES

LIST OF TABLES

ABSTRACT

Climate change is expected to increase both the magnitude and frequency of extreme precipitation events, which may lead to more intense and frequent river flooding. This study evaluated the impact of climate change on water balance components and flood hazard in the Lower Mono river Basin through rainfall- runoff modelling. The projection from two West African Science Service Center on Climate Change and Adapted Land Use (WASCAL) climate model, GFDL-ESM2M and HadGEM2-ES under RCP 4.5 and the hydrological model HBV (Hydrologiska Byråns Vattenbalansavdelning) - light is considered in this study. HBV model was set up for the study area and the modelcalibration and validation was performed against the observed discharge measurments. Statistical bias correction (empirical quantile mapping) was applied to daily precipitation, temperature and evapotranspiration. Uncorrected and bias corrected climate data was then used as input for HBV model to simulate the water balance components. Considering both uncorrected and bias corrected climate variables, the projected climate change signal for the Basin was analyzed through the comparison between two future periods (2020- 2049 and 2070-2099) and the historical time period (1983- 2005). The impact of the detected climate change signal on flood frequency was then assessed using HYFRAN software. The results indicated that: (i) precipitation will increase by 19% and 35%; temperature increases from 0 to 1.17°C and 1.17 to 3.20°C; actual evapotranspiration increase by 9% and 20% and discharge increase by 59% and 102% respectively for the periods 2020-2049 and 2070- 2099 according to HadGEM2-ES model. GFDL-ESM2M model also illustrates an increase in precipitation by 15% and 30%, temperature from 0 to 6.5°C and 6.5°C to 7.41°C but a decrease in discharges by 58% for 2050 and by 44% for 2100 repectively. In case of impact of the climate change signal on flood frequency, the average change resulting from the two models indicated a decrease for the return periods 50, 20, 10, 5, 3 for future periods 2020-2049 and return period 50 for the period 2070-2099 whereas an increase for the return periods 3, 2 (2020-2049) and 20, 10, 10, 5, 3 and 2 (2070-2099).These results suggest for future flood management under climate change in Mono river basin to consider both increase and decrease in the flood frequency as the study shows that both trends are plausible.

Key words: HBV, Climate change signal, Flood frequency, Mono river Basin

RESUME

Les changements climatiques devraient accroître à la fois l'ampleur et la fréquence des événements de précipitations extrêmes, ce qui pourrait entraîner des crues plus intenses et fréquentes. Cette étude évalue l'impact du changement climatique sur les composantes du bilan hydrique et les risques d'inondation dans le bassin inférieur du fleuve Mono à l'aide d'une modélisation pluie-débit. Les projections de deux modèles climatiques GFDL-ESM2M et HadGEM2-ES du Centre de services scientifiques Ouest-Africains sur le changement climatique et l'utilisation adaptée des sols (WASCAL), conformément au RCP 4.5, ont été utilisées pour caler le modèle hydrologique HBV-light (Hydrologiska Byråns Vattenbalansavdelning). Après le calage et la validation du model ainsi que l'évaluation des séries de données historiques générées par les modèles climatiques, une correction statistique des erreurs (cartographie empirique des quantiles) a été appliquée aux précipitations, à la température et à l'évapotranspiration journalières. Les données non corrigées et corrigées ont ensuite été utilisées comme entrée pour le modèle HBV afin de simuler les composantes du bilan hydrique. En tenant compte à la fois des variables climatiques non corrigées et corrigées, le signal de changement climatique projeté pour le bassin a été analysé par comparaison entre deux périodes futures (2020-2049 et 2070-2099) et la période historique (1983-2005). L'impact du signal de changement climatique détecté sur la fréquence des inondations a ensuite été évalué à l'aide du logiciel HYFRAN. Les résultats indiquent pour le signal de changement climatique sur les composantes du bilan hydrique que: (i) les précipitations augmenteront de 19% et 35%; température de 0 à 1,17 ° C et de 1,17 à 3,20 ° C; évapotranspiration réelle de 9% et 20%; débit de 59% et 102% respectivement pour les périodes 2020-2049 et 2070-2099 selon le modèle HadGEM2-ES. Le modèle GFDL-ESM2M illustre également une augmentation des précipitations d'environ 15% et 30%, une température de 0 à 6,5 ° C, puis de 6,5 ° C à 7,41 ° C, mais une diminution des débits de 58% d'ici 2050 et de 44% d'ici 2100. En ce qui concerne l'impact du signal du changement climatique sur la fréquence des crues, la variation moyenne résultant des deux modèles a indiqué une diminution pour les périodes de retour 50, 20, 10, 5, 3 et 50 respectivement pour les périodes futures 2020-2049 et 2070-2099 alors qu'une augmentation pour les périodes de retour 3, 2 (2020-2049) et 20, 10, 10, 5, 3 et 2 (2070-2099). Ces résultats suggèrent qu'une gestion future des inondations sous le changement climatique dans le fleuve Mono prenne en compte à la fois l'augmentation et la diminution de la fréquence des inondations car l'étude montre que les deux tendances sont possibles.

Mots-clés: HBV, Signal du changement climatique, Frequence d'inondation, Basin du Mono

CHAPTER ONE

1. INTRODUCTION

1.1. Background Information

Water, one of the arts for humanity, has always been a key driver of social and economic development. Today the art is becoming more challenging due to the increasing need of people to be protected from water leading to floods (Mujumdar & Kumar, 2012). Flooding occurs when water accumulates in places that are not normally submerged. Flood is the most common form of natural disaster that disturbs human activities, causes loss of human lives and destroy properties (Asumadu-Sarkodie & Owusu, 2016). It occurs when the river water inundates or overflow the land which is generally dry and it impacts human life and socio-economic life and harms the natural environment (Ufe, 2015). The human, material, and ecological costs caused by flooding can be overwhelming for sustainable development.

Flood disasters are caused by either natural factors, such as climate change and climate variability or anthropogenic factors, like socio- economic and land-use developments (Shrestha & Lohpaisankrit, 2016). It has also been reported that flood hazards events will increase under conditions of climate change and put a heavy burden on people's lives, livelihoods and on the economy (Walz & Sassen, 2019). Equally, the effects associated with climate change such as sea level rise, extreme rainfall events, and higher river discharges may be results of this as well.

Many countries all over the world are experiencing heavy rains, rivers overflow, hurricanes, typhoons, tsunamis resulting in unexpected floods which decimate entirely or partly some localities. Based on the Hyogo Framework for Disaster Risk Reduction's, flood statistical data from 1980 to 2008 which have been registered almost 3000 flood events have caused nearly 200,000 deaths, while the economic loss during that same period was US$ 397 billion translating to annual economic loss US$ 13.5 billion (UNISDR, 2005). On the other hand, flood disasters account for half of all deaths caused by natural catastrophes (Ohl, 2000). In 2010, floods were responsible for the loss of more than 8,000 human lives and affected about 180 million people (Guha-sapir, 2010). The devastating floods that occurred in Pakistan, China, Togo, and Benin are some examples. The UN Office for the coordination of Humanitarian Affairs (OCHA) has also

stated that compare with previous years, 2010 has recorded the largest number of people affected and dying from flooding in the world, with Africa being a case in point.

Africa is one of the most vulnerable continents to climate change across the world (Lamboni et al., 2019). The number of people affected by floods in this continent has dramatically increased over the last decades (Guha-sapir, 2010). Extensive urbanization, population growth in natural floodplains, increasing rate of deforestation, are also the key factors that rise the number of people vulnerable to flood (Ramesh, 2012). In 2007, Africa was particularly hit by floods which affected more than two million lives in the central and Eastern parts in January, and 2.6 million victims in a large region from west to east in July and August of the same year (Lamboni et al., 2019).

Changes in climate variables pattern such as precipitation, temperature and evaporation, resulting from climate change, lead to modifications in the global water cycles and affect water resources (Bates, Kundzewicz, & Palutikof, 2008). In addition to the projected changes in these variables, the climate change will also have implications on the extreme events. Studies have shown that flood intensity is highly sensitive to temperature in many parts of the world (Prudhomme et al., 2013). Other studies also have discussed that climate change has been a contributing factor to flood risk by raising the precipitation amount relative to the average annual rainfall (Flemming, Tregoning, Kuhn, Purcell, & McQueen, 2012).Therefore, developing countries, low- income populations are likely to suffer from floods. This is the case for West Africa, one of the regions in the continent that are most vulnerable to climate change (IPCC, 2012). Studies have reported that West Africa experienced above normal precipitation during June – September compared to the last 35 years as a result of the increased overall intensity of the monsoon season (Adegoke et al., 2019). From 1900 till today, over 300 occurrences of climate-related hazards such as flood and droughts have been recorded in West Africa affecting almost 95 million people, displacing roughly two million people and causing about 173,000 casualties, (Walz & Sassen, 2019). Since 1950, flood events caused almost 2,384,437 deaths and about 720 billions of dollars ($) of damages in West Africa.

Many countries in West Africa including Togo, Benin, Ghana, Nigeria, Burkina Faso, Senegal, Ivory Coast have been affected from impacts of devastating flooding in both cities and in rural areas (Ntajal, 2016). From 1900 to 2016, 3,189,547 people have been affected by flood in Benin

and almost 40% of them experienced riverine flood (Houngue, 2018). In 2010, torrential rains and severe flooding hit Benin and Togo. The 2010 flood event is one of the biggest natural disasters recently experienced by both countries. The damage caused by that flooding in Benin amounted to 78.3 billion CFA francs (about USD 160 million) and was related to the total or partial destruction of assets including buildings and inside property, infrastructure, inventory, etc. The losses amounted to 48.8 billion CFA francs, approximately USD 100 million (World Bank, 2011). This resulted in changes in economic flows including production deficits and unrealized sales. As for Togo, according to "EM- DAT" (Emergency Events Database) of the Centre for Research on the Epidemiology (CRED), the 2010 flood has impacted both urban and rural areas throughout the entire country, affecting 82,767 people; causing damages and losses amounted to an estimated 1.1 percent of GDP. Many urban and rural areas located within the Mono River Basin, the largest river shared between Togo and Benin were hit almost every year by floodings which were caused by the overflow of the River. The previous flood events occurred in 2007, 2008 and 2018 in Togo have also caused a lot of damages and loss to people living in areas located in the Mono River Basin (Ntajal et al., 2018).

1.2. Problem statement

Flood event has many effects on economic, social and environmental aspects which are useful to achieve the sustainable development goals and it is taken to be the best common and extremely destructive of all hazards and also predicted to become more frequent, dominant and serious in the coming year generally in the growing towns (Mureithi et al., 2015). The vulnerability with these natural risks is high in West Africa and Togo and Benin in particular, where the populations living in the Mono River Basin tend to occupy the most exposed zones, (Fernando, 2014). Ntajal (2016) has identified that most of the communities in the lower basin of Mono river were within a 500 meter buffer zone while others such as Agbanakin, Togbavi, Azime Dossou, and Adame were found within 100 m, which could increase their exposure to flooding, (Ntajal, 2016), Figure 1.

From the section 1.1; It has been shown that Mono River Basin is getting flooded each year and the areas located in the downstream suffer the impact of its overflow. Past and recent scientific researches undertaken in the Basin focused more on Flood characteristics, flood risk and vulnerability (Ago et al., 2005; Amoussou, 2010; Fernando, 2014; Ntajal, 2016).

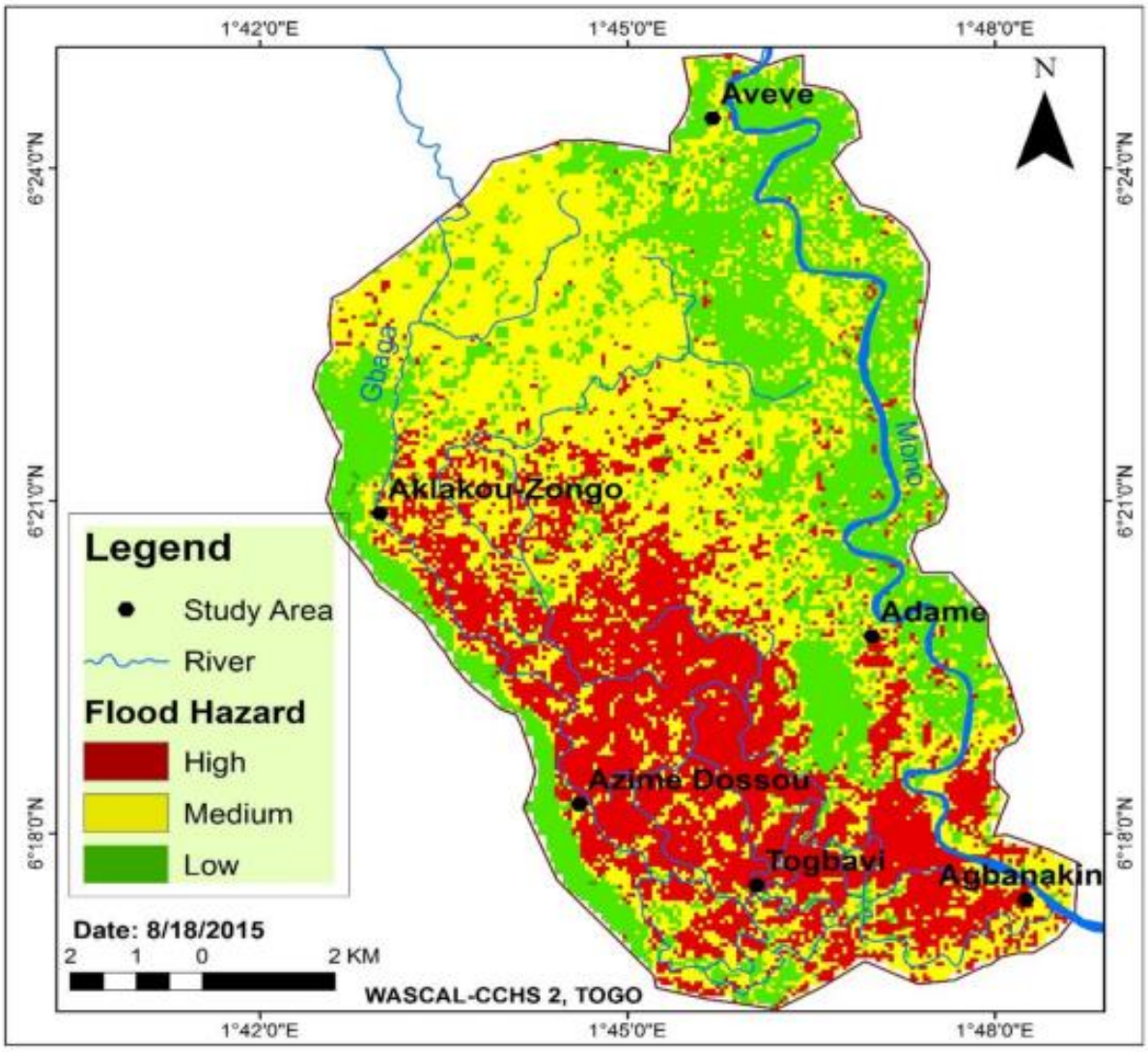

Figure 1. Flood hazard map of the Lower Mono river basin (Lacs district), (Ntajal, 2016)

However, little work has been focused on the impacts of climate change. For instance, Houngue (2018) investigated the impact of climate change on Mono river inflow while Lamboni et al. (2019) assessed the rainfall trends and changes over Mono River Basin using Africa- CORDEX regional climate models under the Representative Concentration Pathways, RCP 8.5. Ntajal (2016) evaluted the flood risk in the lower Mono River. His findings also showed that the lower part of Mono River Basin is likely to be mostly affected by 2-year and 5- year flood. None of these studies performed flood frequency analysis of annual maximal discharge derived using climate scenarios and hydrological model. This research comes to fill this gap by applying the HBV-light model (Hydrologiska Byråns Vattenbalansavdelning), to assess the impact of climate change on flood frequency and magnitude, using two West African Science Service Center on Climate Change and

Adapted Land Use (WASCAL) climate model output (GFDL-ESM2M and HadGEM2-ES under RCP 4.5).

1.3. Research Objective

1.3.1. Main Objective

The overall objective of our research is to evaluate the impact of climate change on water balance components and flood hazard in Mono River through rainfall - runoff modelling.

1.3.2. Specific objectives

The specific objectives are to:

- Calibrate and validate the hydrological model HBV for the Lower Mono river basin;
- Evaluate the climate change signal on water balance components in the Mono river;
- Assess the impact of Climate Change (CC) on flood frequency and magnitude in the Mono River.

1.4. Research questions

Based on the stated objectives, the following questions have been used to guide the research process and finally answered from the findings of the study:

- How well could the HBV model perform in simulating discharge over the Lower Mono River?
- What could be the signal of climate change on water balance components of the lower Mono River?
- How does climate change impact on flood frequency in Mono, lower basin?

1.5. Relevance of the study

The Fifth Assessment Report (AR5) by the Intergovernmental Panel on Climate Change (IPCC, 2014) highlighted that flooding in West Africa are expected to increase by 20% over the next decades relative to the past (1986-2005) due to the impact of climate change which is likely to become more severe by 2050. It is thus, understood that flood risks in Mono River Basin will not subside in the future (Lamboni et al., 2019). This study is therefore welcome to assess the local beheviors of climate change impact on flood hazard in Mono lower Basin. It is also a step forward for better management of flood in the region. As Mono Basin is one the largest Basin shared between both Benin and Togo countries, the output of this study will also help stakeholders and decisions makers to plan and adopt strategies in order to prevent or to mitigate the incoming impact of flood in both countries through the Mono River Basin.

1.6. Thesis Outline

The outline of this thesis report is composed of five chapters and is as follows:

- The first chapter provides the introduction of this study: it includes the background, the problem statement, the objectives of the study, the research questions and justification of the study.
- The second chapter provides a literature review which illustrates the state of the art as far as studies climate impact on flood are concerned.
- The third chapter presents the description of the study area.
- The fourth chapter provides research methodology, the data used for this study with discussion on their pre-processing.
- The fifth chapter presents the results and discussion.
- The sixth chapter provides a conclusion and few suggestions.

CHAPTER TWO

2. LITERATURE REVIEW

2.1. Hydrological modeling

2.1.1. A general overview of Hydrological modeling

A model can be defined as a simplified representation of a real-world system (Gayathri, 2015). Models are used for predicting system behavior and understanding various hydrological processes. The model giving results close to reality with the use of the least parameters is the best one. Hydrological models are an important tool for water and environment resource management.

A large number of hydrologic models are available today with varying degrees of data requirements that may be used for purposes such as estimation of flood runoff, routing of flood hydrographs, and assessment of flood inundation, which may be done with a GIS interface (Icyimpaye, 2018).

Hydrological modeling is the use of physical or mathematical techniques to simulate the hydrologic cycle and its effect on a watershed. The purpose of using a model is to establish baseline characteristics whenever data is not available and to simulate long-term impacts that are difficult to calculate (Mkilima, 2018).

Hydrologic models attempt to simulate the rainfall-runoff process to tell us "how much water, how often". They use rainfall information or simulations to provide runoff characteristics including peak flow, flood hydrograph and flow frequencies (Georgia stormwater Management Manual G-1). The hydrological model can be classified as a lumped and distributed model based on the model parameters as a function of space and time; deterministic and stochastic models based on the other criteria (Gayathri, 2015).

In lumped models, the entire river basin is taken as a single unit where spatial variability is disregarded. The output is then generated without considering the spatial processes. As for a distributed model, it can make predictions that are distributed in space by dividing the entire basin into small units, mostly square cells or triangulated irregular network, therefore the parameters, inputs, and outputs can vary spatially.

The semi-distributed models account for spatial variations in some processes while ignoring them in others by dividing the basins into a number of smaller sub-basins. On the time scale, the models may be discrete or continuous time models.

With the deterministic model, the same output is obtained for a single set of input values while in stochastic models, different values of output can be produced for a single set of inputs.

One of the most important classifications is an empirical model, conceptual models and physically based models (Gayathri, 2015).

- Empirical models also called data-driven models are observation oriented models which take only the information from the existing data without considering the features and processes of the hydrological system. Artificial neural network and fuzzy regression, are some of the empirical models.
- The conceptual model describes all of the component hydrological processes. Semi-empirical equations are used in this model and the parameters are assessed from the field data and through calibration. A large number of meteorological and hydrological records is required for calibration. HBV model and TOPMODEL are some examples of this model.
- Physically based model is a mathematically idealized representation of the real phenomenon. It does not require extensive hydrological and meteorological data for their calibration but the evaluation of a large number of parameters describing the physical characteristics of the basin are required. This model requires a huge amount of data such as soil moisture content, initial water depth, topography, topology, dimensions of the river network, etc. are required. SHE or MIKESHE model and SWAT are some of this model.

2.1.2. Brief description of the HBV model and applications

As the main goal of the hydrological modeling in this research is to simulate peak flow, any model which can simulate that characteristic of Mono river could be used. However, this study used, HBV-light model (Hydrologiska Byråns Vattenbalansavdelning, (Seibert, 2005), version 4.0.0.22 which has many characteristics among which simple structure, conceptual, lumped, requires a moderate amount of input data. HBV is part of IHMS (Integrated Hydrological Modeling System) and is used for hydrological prediction, discharge simulation, and flood analysis under climate change (Houngue, 2018). The HBV-light is a conceptual, lumped model of basin hydrology which simulates daily discharge using daily rainfall, temperature and estimates of potential evapotranspiration (PET) as input data (Radchenko, 2016).In-depth details and descriptions on the model are available (Harlin, 1992; Lindström & Harlin, 1992; Seibert, 1997).

The HBV model (Bergstrom 1976) has been applied in numerous studies, e.g., to do hydrological forecasts, for the computation of design floods or for climate change studies (Bergstrom 1992).

Many ongoing researchers are there on topics like which model will give more compatible results with that of observed discharges. Gayathri (2015) made a review on hydrological models such as Variable Infiltration capacity model (VIC), TOPMODEL, HBV, MIKESHE and Soil and Water Assessment Tool (SWAT) model. His findings show that HBV model can be used for flood forecasting and many other purposes.

Grillakis et al. (2010) also used the HBV model in a flash flood case in Slovenia and it gives satisfactory results, the coefficient of determination r^2 ranged between 0.86 and 0.92; The coefficient of efficiency, R_{eff} varied from 0.82 to 0.90 during calibration; as for validation, $\mathbf{r^2}$ varied between 0.58 and 0.79 , and R_{eff} ranged from 0,69 to 0.90 . Radchenko (2016) used HBV-light model to study "Impact of climate change on the contribution of second order tributaries to the water balance of the Ferghana Valley". His findings show that "the HBV-light model is successfully applied in the study area and it shows the capability to capture the main peaks of discharge and to simulate the base flow both for generated and measured temperature data, as well as to reproduce the observed discharge time series".

HBV model has been also used in Benin for different researches. Among them, Bormann and Diekkrüger (2003) applied the HBV model to predict discharge in the Upper Ouémé Basin. The model was also used in the Mekrou Basin to simulate various parts of hydrograph over the period 2004- 2011 (Gaba et al., 2015). The impact of climate change on blue and green water in the Niger River Basin, Benin was assessed using HBV-light model (Badou, 2016).

Houngue, (2018) also used HBV-light while assesing the impact of climate change on Mono River discharge by 2050. The hydrological model, HBV-light was used to simulate future discharge using the projections from the regional climate model REMO, under RCP4.5 and RCP 8.5. The coefficient of efficient of efficient was 0.79 during calibration and 0.67 during validation while r^2 reached 0.83 and 0.73 respectively in calibration and validation.These values study showed that HBV-light is able to well-simulate discharge in the Mono Basin over the period 1980- 2010 and 2018 -2050.

- HBV-light model structure

As shown by figure 2 and figure 3, the model includes four different routines: snow, soil, groundwater (response function) and routing. The snow routine is based on a degree-day method, where precipitation is considered to be rain or snow with respect to a threshold temperature, TT (°C) (Lindström et al. 1997; Seibert and Vis 2012; Seibert et al. 2000). The soil routine simulations depend on actual evaporation and water storage properties (Seibert et al. 2000; Seibert 1997). The groundwater routine is governed by percolation rate (PERC) and recession coefficients (K1, K2), (Seibert 1997; Seibert and Vis 2012). Finally, the runoff generation is characterized by the shape of a triangular weighting function (Lindström et al. 1997; Seibert et al. 2000).

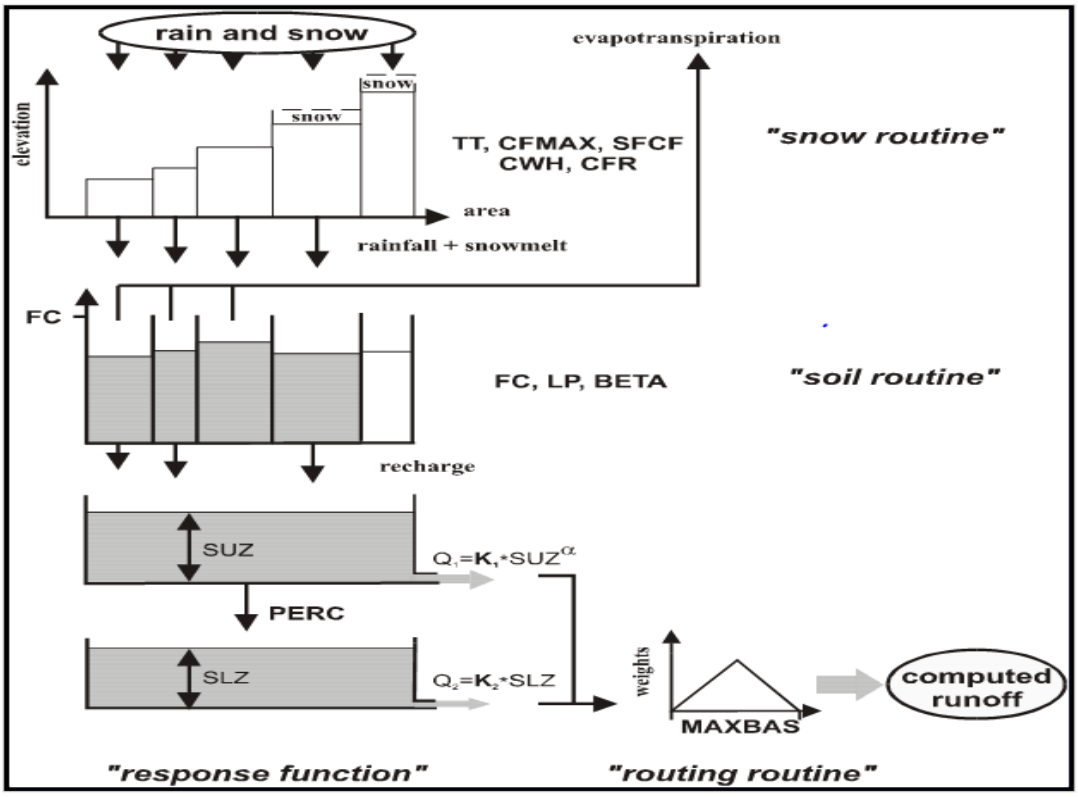

Figure 2. The general structure of HBV model

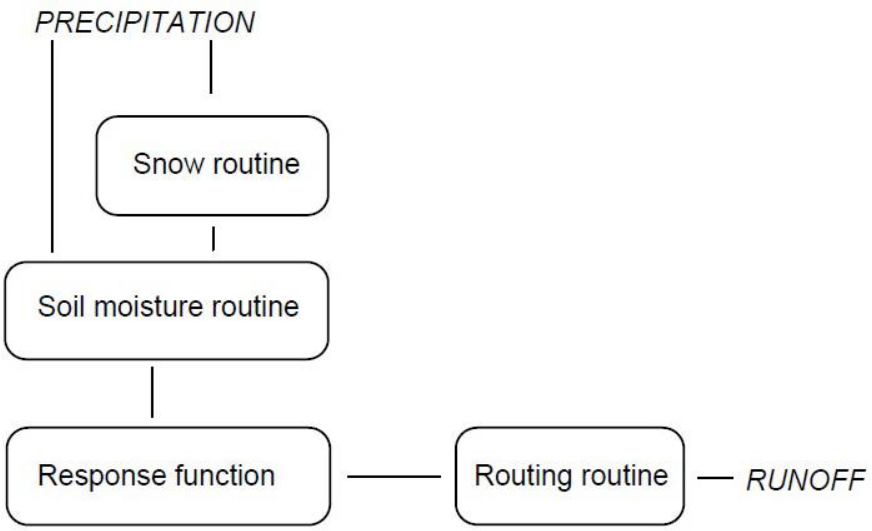

Figure 3. The schematic model structure

The four sub-models of HBV-light deal with different aspects of water balance.

Table 1, summarized the input and output data as well as the parameter of each routine.

The response function is built upon a single linear reservoir model. where the runoff Q(t) at time t is supposed to be proportional to the water storage S(t).

$$Q(t) = K * S(t) \quad \textbf{(1)}$$

Where Q (t) is the runoff at time t, S (t) the water storage, K is the storage (or recession) coefficient and t is the time

$$S(t) = SP + SM + Suz + Slz + Lakes \quad \textbf{(2)}$$

Where SP is the snow pack, SM the soil moisture, Suz upper groundwater zone, Slz lower groundwater zone and Lakes the volume of lakes.

The water balance of the Basin is given by:

$$P(t) = E(t) + Q(t) + \frac{ds(t)}{t} \quad \textbf{(3)}$$

Where P(t) is the precipitation, E(t) the evapotranspiration, Q(t) the runoff at time t.

The general structure of HBV-light, considers the soil as divided into two boxes, the upper groundwater zone Suz, and the lower groundwater zone Slz, and the flow from groundwater boxes, $Q_{WG}(t)$ is:

$$Q_{WG}(t) = K2.Slz + K_1.Suz + K_0.\max(Suz - UZL, 0) \quad \textbf{(4}$$

Where Slz is the recharge added to the lower groundwater box, Suz the recharge added to the upper groundwater box, ULZ a threshold parameter, K_0, K_1, K_2 the storage (or recession) coefficient. Then, the simulated streamflow, Q_{sim}, is obtained by applying a triangular weighting function defined by the parameter MAXBAS.

$Q_{sim}(t) = \sum_{i=1}^{MAXBAS} c(1).Qwg(t-i+1)$ **(5)**

Where $c(i) = \int_{i-1}^{i} \frac{2}{MAXBAS} - \left|u - \frac{MAXBAS}{2}\right| . \frac{4}{MAXBAS^2} du$ **(6)**

Table 1. HBV-light sub- models, (Houngue, 2018)

Sub-model	**Imput data**	**Output data**	**Parameter**
Snow routine	Precipitation; Temperature	Snow pack; Snow -melt	TT= treshold temperature (°C); CFMAX= degree-Δt factor (mm °C Δt^{-1}) ; SFCF = snowfall correction factor (-); CFR= refreezing coefficient (-); CWH= water holding capacity (-)
Soil Routine	Potential evapotranspiration ; Precipitation; Snowmelt	Actual evapotranspiration ; Soil moisture; Groundwater recharge	FC= maximum soil moisture storage (mm); LP= soil moisture value above which AET reaches PET (mm); BETA= parameter that determines the relative contribution to runoff from or snowmelt (-)
Response function	Groundwater recharge; Potential evapotranspiration	Runoff; Groundwater level	PERC= threshold parameter (Δt^{-1}); Alpha= non-linearity coefficient (-); UZL= threshold parameter (mm); K= storage (or recession) coefficient (Δt^{-1})
Routing routine	Runoff	Simulated runoff	MAXBAS= Length of triangular weighting function (Δt)

Among the 14 parameters which HBV-light has, only 8 are taken into consideration in this study, because the remaining five govern the snow routine and are not relevant for Mono Basin. The same number of parameters were considered in the study of "assessment of mid-century climate change impacts on mono river's downstream inflows" (Houngue, 2018).

2.1.3. Data processing and Model set-up

2.1.3.1. Data requirement

The reliability of hydrological models is highly dependent on the calibration procedure, which is the search for one optimal parameter set (Gayathri, 2015).

HBV model requires some data files which should be prepared before inputting them in the model. Those data files are PTQ-files and Evaporation-file.

- PTQ-files: The PTQ-file contains time series of daily precipitation (mm/day), temperature (°C) and discharge (mm/day), (Seibert, 2005).
- Evaporation-file: The evaporation-file contains values for the potential evapotranspiration (mm/day). The evaporation file may contain 12 values, i.e. long-term monthly mean values or 365 values, i.e. long-term daily mean values, (Seibert, 2005).

2.1.3.2. Calibration

The model calibration is a systematic process of adjusting the model parameter values until model results match acceptably with the observed data. This involves obtaining the best match between the observed and the computed discharge hydrographs.

The calibration of a conceptual model such as HBV model, basically follows two approaches: the first is usually made by a manual try and error technique while the second is an automatic fitting using an optimization algorithm.

Some automatic calibration tools are available in HBV model: Monte Carlo runs and the genetic calibration algorithm (GAP optimization). The latter is used in this study for model calibration.

During the calibration, relevant parameter values are changed until an acceptable agreement with observations is obtained.

Some criteria can be applied to analyze the fit of simulated discharge or runoff to the observed one (Bergström, 1992):

- Visual inspection of plots with Simulated discharge (Qsim) and Observed discharge (Qobs)

- Accumulated difference: it is a graph of the accumulated difference between the simulated and the record discharge or runoff which reveals any bias in the water balance and is particularly useful in the initial stage of calibration, for example for assessment of snow-fall corrections.
- Statistical criteria, normally the R_{eff} –value according to Nash and Sutcliffe (1970).

The coefficient of efficiency, R_{eff}, is normally used for assessment of simulation by the HBV model (Bergström, 1992). R_{eff} is the objective function used for the HBV model calibration in the present work.

$$R_{eff} = 1 - \frac{\sum(Qsim(t) - Qobs(t))^2}{\sum(Qobs(t) - \overline{Qobs})^2} \quad (7)$$

R_{eff} compares the prediction by the model with the simplest possible prediction, a constant value of the observed mean value over the entire period.

R_{eff} =1, Perfect fit, if the simulation and the observations agree completely;

$$QSim(t) = QObs(t). \quad (8)$$

R_{eff} =0, Simulation as good (or poor) as the constant –value prediction if the model does not perform any better than the mean value of the discharge record.

R_{eff} <0, Very poor fit, if the model performance is poor or poor data is used.

2.1.3.3. Model Validation

It is the process of testing the ability of the model to simulate observed data other than that used for calibration, with acceptable accuracy. In other words, the validation tests the performance of the model with calibrated parameters for an independent period.

2.1.3.4. Performance evaluation of the model

Various goodness of fit functions is available in HBV-light model:

- Reff: model efficiency
- ReffWeighted: Efficiency based on weighted Q
- LogReff: Efficiency for log (Q)
- r^2: coefficient of determination
- MeanDiff: Mean difference

- VolumeError: Volume error
- FlowWeightedReff: Flow-weighted efficiency
- Kling-Gupta efficiency (KGE)

Among them, efficiency criteria frequently used for hydrological applications and flow comparisons such as Nash-Sutcliffe efficiency, coefficient of determination (Grillakis et al.,2010) were used for this study.

In addition, Kling-Gupta efficiency was also taken into consideration. In fact, taking into account multiple objectives can reduce simulation uncertainties and provides more reliable predictions. The Kling-Gupta model efficiency is in line with the paradigm of using many objectives during the calibration of the model in order to prevent the overfitting of model parameter to a particular hydrograph aspect (Pool et al., 2018).

Therefore, these criteria are used to evaluate the model simulations during the calibration and validation periods.

- **Coefficient of determination r^2**: it is defined as the squared value of the coefficient of correlation according to Bravais-Pearson ((M G Grillakis et al., 2010). The coefficient of determination indicates the correlation between the observed and simulated values. It is calculated as follows:

$$r^2 = \frac{\left(\sum(Qobs-\overline{Qobs})(Qsim-\overline{Qsim})\right)^2}{\sum(Qobs-\overline{Qobs})^2 \sum(Qsim-\overline{Qsim})^2} \quad \textbf{(9)}$$

- **The efficiency E (R_{eff}):** proposed by Nash and Sutcliffe (1970) is defined as one minus the sum of the absolute squared differences between the predicted and observed values normalized by the variance of the observed values during the period under investigation. *E* measures how well the plot of the observed against the simulated flows fits the 1:1 line. The range of E lies between 1.0 (perfect fit) and -8. A result lower than zero indicates that the mean value of the observed time series would have been a better predictor than the model. It is calculated as shown in formula 1, section 2.3.1.
- **Kling-Gupta efficiency (KGE):** it provides a way to achieve balanced improvement of the simulated mean flow, flow variability (high flow estimates), and daily correlation through. KGE is a weighted combination of three components that appear in the theoretical NSE decomposition formula and showed that this formulation improves flow variability estimates (Mizukami et al., 2018).

KGE is expressed as:

$$KGE = 1 - \sqrt{\{Sr(r-1)\}^2 + \{S\alpha(\alpha-1)\}^2 + \{S\beta(\beta-1)\}^2} \quad \textbf{(10)}$$

Where, $\alpha = \frac{\sigma s}{\sigma o}$, $\beta = \frac{\mu s}{\mu o}$ **(11)**

where Sr, $S\alpha$ and Sβ are user-specified scaling factors for the correlation (r), variability ratio (α), and mean ratio (β) terms; σs and σo are the standard deviation values for the simulated and observed responses respectively, and μs and μo are the corresponding mean values. In a balanced formulation, Sr, $S\alpha$ and $S\beta$ are all set to 1.0. By changing the relative sizes of the Sr, $S\alpha$ and $S\beta$ weights, the calibration can be altered to more strongly emphasize the reproduction of flow timing, statistical variability, or long-term balance (Mizukami et al., 2018).

2.1.4. Areal precipitation

There are different methods to compute the average rainfall in areas where more than one rain gauge is established:

- Arithmetic average method
- The weighing means method or Thiessen polygon method
- Kriging method
- Isohyetal method.

In this study, Thiessen polygon and Kriging ordinary were considered.

2.1.5.1. Thiessen Polygon method

It is the weighted mean method. The rainfall is never uniform over the entire area of the basin but it varies in intensity and duration from place to place. The rainfall recorded by each rain gauge station should be weighted according to the area, it represents.The Thiessen polygon method is more suitable under the following conditions: for areas of moderate size; when rainfall stations are few compared to the size of the basin; in moderate rugged areas. The following procedure is used to apply thiessen polygon method: Draw the area concerned to a suitable scale, showing its boundary, locations of the rain gauges in the area and outside but close to the boundary; Join the location of the rain gauges to form a network of triangles; Draw perpendicular bisectors to the triangle sides. These bisectors form polygons around the stations; Delineate the formed polygons and measure their areas using a planimeter or by converting them into smaller regular geometric shapes (i.e.triangles, squares, rectangles, etc.). Compute the average rainfall using the following formula:

$$P_{av} = \frac{P1xA1 + P2\ xA2 + \ldots + PnxAn}{A1 + A2 + \cdots An} \quad \textbf{(12)}$$

Where, P_{av} the average rainfall and A1, A2…An the area of each polygon

2.2. Climate change

2.2.1. Global Circulation Model

Global or general circulation models (GCM) are large scale numerical models of the atmosphere and ocean circulation. They use hydrodynamic (Navier-stokes equations on Rotating sphere) with thermodynamics (radiation and latent heat) coupled together with atmospheric, ocean and other modeled aspects of the climate system to form a global climate model or earth system, model.

GCMs simulates the Earth's climate system over time to compute atmospheric water vapor, ocean temperatures, greenhouse gas concentrations, annual and daily solar heating and describe how these components interact with each other to create complex climate variability and change (ARCC, 2014).

They are the main tools used to provide a reasonably accurate representation of global and continental scale climate information on average daily, monthly, seasonal, annual and longer time scales used for forecast and projection of impacts of anthropogenic greenhouse gases (GHGs) and aerosols on future climate.

2.2.2. Representative Concentration Pathways (RCP)

The Representative Concentration Pathways (RCP) is the latest generation of scenarios that provide input to climate models. RCPs are time and space dependent trajectories of concentrations of greenhouse gases and pollutants resulting from human activities, including changes in land use. The four RCPS are:

- **RCP 8.5: High emissions: -** consistent with a future with no policy changes to reduce emissions. Comparable SRES scenario: A1 F1
- **RCP 6: Intermediate emissions: -** consistent with the application of a range of technologies and strategies for reducing greenhouse gas emissions. Comparable SRES scenario: B2.
- **RCP 4.5**: **Intermediate emissions: -** consistent with a future with relatively ambitious emissions reductions. Comparable SRES scenario: B1
- **RCP 2.6**: **Low emissions**: - In order to reach such forcing levels, ambitious greenhouse gas emissions would be required over time.

2.2.3. An overview of WASCAL Climate models

WASCAL is a big research-focused Climate Service Centre in West Africa that enhances the resilience of human and environmental systems to climate change and increased variability in the region of West Africa. Within the framework of the West African Science Service Center on Climate Change and Adapted Land Use (WASCAL), an ensemble of high-resolution regional climate change scenarios for the greater West African region is provided to support the development of effective adaptation and mitigation measures. Three regional climate models (WFR V 3.5.1, COSMO-CLM 4.18, REGCM4) and three earth system models from the CMIP5 project are downscaled by each of the regional models, MPI-ESM, GFDL-ESM2M and HadGEM2-ES over the period of 1980 - 2010.

GFDL-ESM2M and HadGEM2-ES data were downloaded from the Earth System Grid Federation (ESGF) in netCDF format. For GFDL-ESM2M and HadGEM2-ES data, a separate tool were implemented to convert the netCDF data directly into the WPS intermediate format ("un-netcdf"), thereby avoiding the problem of an unsupported 360-day calendar in the grib standard.

To generate model output in a standard format, the latest developments in the WRF model were employed and extended further: WRFV3.5.1 provides the capability to interpolate model-level data to pressure levels during the integration. This capability was extended to include additional variables (in particular hydrometeors). Further, climate diagnostics such as minimum and maximum daily temperatures are calculated using the climate diagnostics features of the model.

The GFDL-ESM2M and HadGEM2-ES models are based on a 365-day (no-leap year) and a 360-day (12×30 days) calendar, respectively.Regional climate projections are generated at high (12 km) and intermediate (60 km) resolution using the Weather Research and Forecasting Model (WRF). The simulations cover the validation period 1980–2010 and the two future periods 2020–2050 and 2070–2100. The high spatial and temporal resolution of the data, the extensive list of output variables, the large computational domain and the long time periods covered make this data set a unique resource for follow-up analyses and impact modelling studies over the greater West African region.

The Representative Concentration Pathways considered in the simulation is the RCP4.5 scenarios from 2020 to 2050 and from 2070 TO 2100. The choice of RCP4.5 was made because of limited computational resources and is based on the fact that the differences between RCP4.5 and RCP8.5 become apparent only after 2040 (Heinzeller et al., 2018). The selected GCMs, on the other hand,

cover the extremes in temperature and precipitation of the ensemble of GCM forcing data used in CORDEX. The simulation outputs are provided at the resolution of 12km and 60km. It is covering all west Africa region from 25W to 25E and 5S to 25N (Heinzeller et al., 2018).

2.2.4. Bias correction and Quantile mapping method

Climate model output provides the primary source of information used to quantify the effect of the foreseen anthropogenic climate change on natural systems. One of the most common and technically sound practices in climate change Impact (CCI) studies is to calibrate impact models using the most suitable observational data and then to replace them with the climate model data in order to assess the effect of potential changes in the climate regime (Grillakis et al., 2017). Raw climate model data cannot often, be used in CCI models due to the presence of biases in the representation of regional climate (Christensen et al., 2008). Hydrological Climate Change Impact studies results have been reported to become unrealistic without a prior adjustement of climate forcing bias (Hagemann et al., 2013; Harding et al., 2014; Ines & Hansen, 2006; Sharma et al., 2007). These biases are attributed to a number of reasons such as the imperfect representation of the physical processes within the model code and the coarse spatial resolution that does not permit the accurate representation of small-scale processes. A number of statistical bias correction methods have been developed and successfully applied in CCI studies (Grillakis et al., 2013; Ines & Hansen, 2006; Teutschbein & Seibert, 2012). Their objective is to adjust the statistical properties of climate simulations to resemble those of observations, in a common climatological period. A commonly used procedure to achieve this is a transfer function (TF) which minimizes the difference between the cumulative density function (CDF) of the climate model output and that of the observations, a process also referred to as quantile mapping. As a result of quantile mapping, the reference (calibration) period's adjusted data are statistically closer, and sometimes near-identical to the observations.

The quantile mapping method (Gudmundsson et al., 2012; Ines & Hansen, 2006; Themeßl et al., 2011; Wood et al., 2004) is a relatively simple approach that has been successfully used in hydrologic and climate impact studies (e.g., Brocca et al., 2011; Cayan et al., 2008; Hayhoe et al., 2004; Maurer & Hidalgo, 2008). In the Niger river basin (West-Africa), Oyerinde (2016) used quantile mapping for precipitation and delta-change for temperature data from 8 RCMs, and concluded the methods as suitable for improving the data. In the Ouémé basin (Benin), N'Tcha M'Po et al., (2016) investigated the linear scaling, the delta approach and the quantile mapping

methods for correcting precipitation data from 4 RCMs and stated that empirical and adjusted quantile mapping are the most effective. Teutschbein and Seibert, (2012) proved that compared to other bias correction method, quantile mapping performs best in terms of hydrological annual maximum simulations. The same conclusions have been drawn by Themeßl et al., (2011) who, comparing several downscaling approaches, indicated the quantile mapping method as the most efficient in removing precipitation biases, also for the tails of the probability density function. Through the quantile mapping, the mapping of the Global Circulation Model cumulative distribution function (CDF) of the variable of interest onto the observed CDF is done.

2.3. Flood Frequency analysis

2.3.1. An overview of Flood frequency analysis

Flood frequency analyses enable predictions of possible flood magnitude over a certain period and to estimate the frequency with which floods of a certain magnitude may occur. The flood frequency analysis is one of the important studies of river hydrology, which could be conducted based on maximum instantaneous flow (Ntajal, 2016).

There are three steps in frequency analysis (Khaliq et al., 2006)

- selecting a suitable Probability Distribution Function (PDF);
- estimating the parameters of PDF based on samples;
- assessing the uncertainty of objective of interest in prescribed confidence level.

Flood frequency analysis is the procedure of obtaining the relationship between flood quantiles and their non-exceedance probability using extreme value theory.

The magnitude of the T-year flood at a site is the amount of streamflow that has a probability 1/T of being exceeded in any one year.

- Using either the Annual Maximum Series (AMS) or Peak Over Treshold (POT) methods/ Partial Duration Series (PDS), a selection of values from the streamflow series can be considered peak events (Claps & Laio, 2003).

Figure 4 presents the general approach in flood frequency analysis using streamflow series.

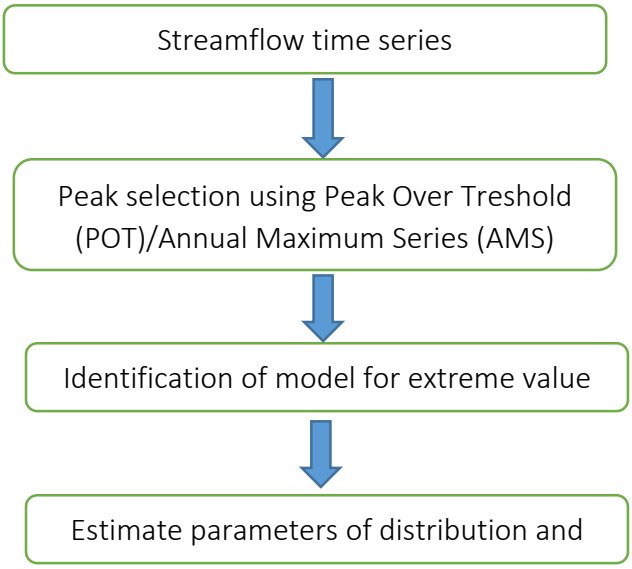

Figure 4. Flood frequency analysis flow chart

In this study, one of the most common approach used, Annual Maximum series were applied to select the peak from the streamfow times series.

2.3.2. Probability distribution

For accurate hydrologic analysis of flooding there are different probability distributions method used to estimate extreme rainfall such as Beta –P; Generalized extreme value(GEV), Gumbel, Weibull, Beta-k, Generalized Logistic (GLO), Generalized Pareto(GPA), Log-Pearson Type III, Pearson Type III and Generalized Normal,GNO, (Icyimpaye, 2018).

The generalized extreme value (GEV), of which extreme value type I (EV I), EV II, and EV III are special cases, and the generalized Pareto distribution (GDP) are frequently used when analyzing data in the context of extreme value theory (Ghorbani, Ruskeep, Singh, & Sivakumar, 2010). The EV I or Gumbel distribution is commonly used for the distribution of annual maxima of streamflows, though the Person type 3 or log-normal is also common. It is indeed the most widely used distribution to model extremes in hydrology (Koutsoyiannis, 2004). The EV III distribution is used for annual low flows.The most common approaches are the annual maximum series (AMS) method and the Peak-over-threshold (POT) or Partial duration series (PDS) method. Among the many probability distributions, the ones that are commonly used are Pearson type III, Weibull, Generalized Extreme Value distributions, Gumbel which seem to adequately fit peak, rainfall and stream-flow (Ghorbani et al., 2010).

2.3.3. Parameter Estimation Method

There is a multitude of methods for estimating parameters of hydrologic frequency models. Some of the popular methods used in hydrology include

- method of moments;
- method of probability weighted moments;
- method of mixed moments;
- L-moments;
- maximum likelihood estimation;
- least squares method.

Extensive details of these methods are already available in the literature (e.g., Rao & Hamed, 2000; Singh, 1996) and, therefore, are not reported here. Only two 2 of these methods are employed: maximum likelihood estimation and the method of moiments. There is no specific reason for preferring these 2 methods against the others, except that they are simple and also sufficient for the purpose of this study. They are neither treated as superior to the other methods nor any effort is made compare with them. Parameter estimation methods commonly used are the method of moments, probability-weighted moments or L-moments, or maximum likelihood.

2.3.4. HYFRAN Software

The HYFRAN software is designed for Hydrological Frequency Analysis (HFA) especially for extreme value. HYFRAN sotware version 1.1 (Salaheddine & Bobée, 2015) is the one used in this study. It is a tool developed by Canadian Developer used to fit statistical distributions (Alib et al., 2016). For flood analysis, the maximum annual flow is often considered. However, HYFRAN allows to fit different statistical distributions (

Figure 5), to any dataset of extreme values in areas with different time steps, provided that observations are Independent and Identically Distributed (IDD). The “comparison” option allows to compare several fittings to choose which is the most adequate to represent the studied dataset. The fittings can be compared using criteria or graphics.

Graphic: It is possible to compare the results of several different fits (2 or 5) using either Normal or Gumbel probability paper.

Criteria: Two criteria are available, these are the Akaike (AIC) and Bayesian information Criteria (BIC) (see Ehsanzadeh et al., 2010).Criteria can be reliably used in climate statistics to assist in finding the best distribution to use to fit the given data. These tests describe the differences between

the observed data values, and the expected values from the distribution being tested (Millington, Das, & Simonovic, 2011).

Model selection is performed by looking for the minimum AIC and BIC values. The probability distribution recording the lower AIC and BIC is the best fitting the data series (Giuliano, Laio, & Montanari, 2009).

$$AICj = -2ln(Lj) + 2pj \quad \textbf{(13)}$$

Where pj is the number of estimated parameters, and Lj is the likelihood function and n is the sample size.

The Bayesian criterion (BIC) is based on the discrepancy between the model and the parent distribution in a Bayesian framework (Schwarz, 1978). BIC can be computed according to the following relationship:

$$BIC = -2\,ln(Lj) + ln(n)pj \quad \textbf{(14)}$$

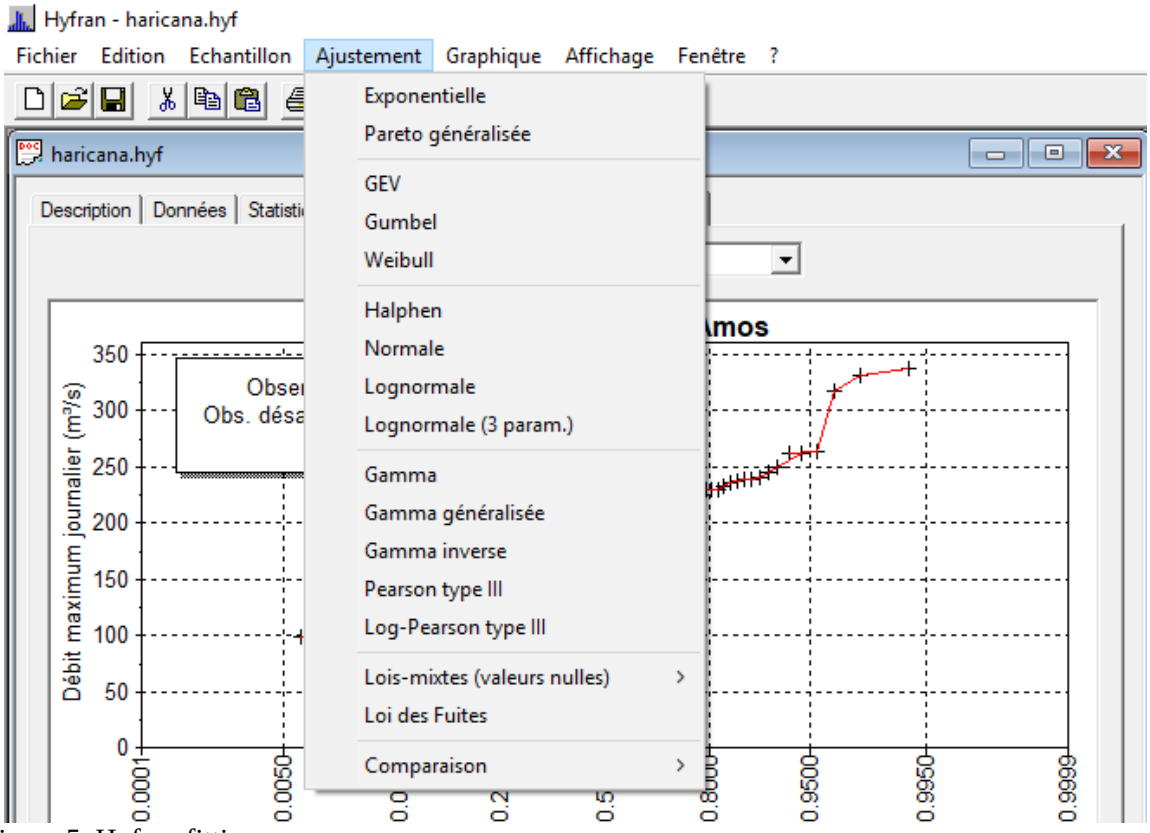

Figure 5. Hyfran fitting menu

CHAPTER THREE

3. STUDY AREA

This section describes briefly the characteristics of the study area which include basin location, population and economics activities; topography, vegetation and soil and the climate.

3.1. An Overview of the Basin

The Mono river basin is located in the Gulf of Guinea region and is shared between Benin and Togo. The upper and middle parts of the basin are largely located in Togolese territory and the lower course lies between Togo and Benin (figure 6).

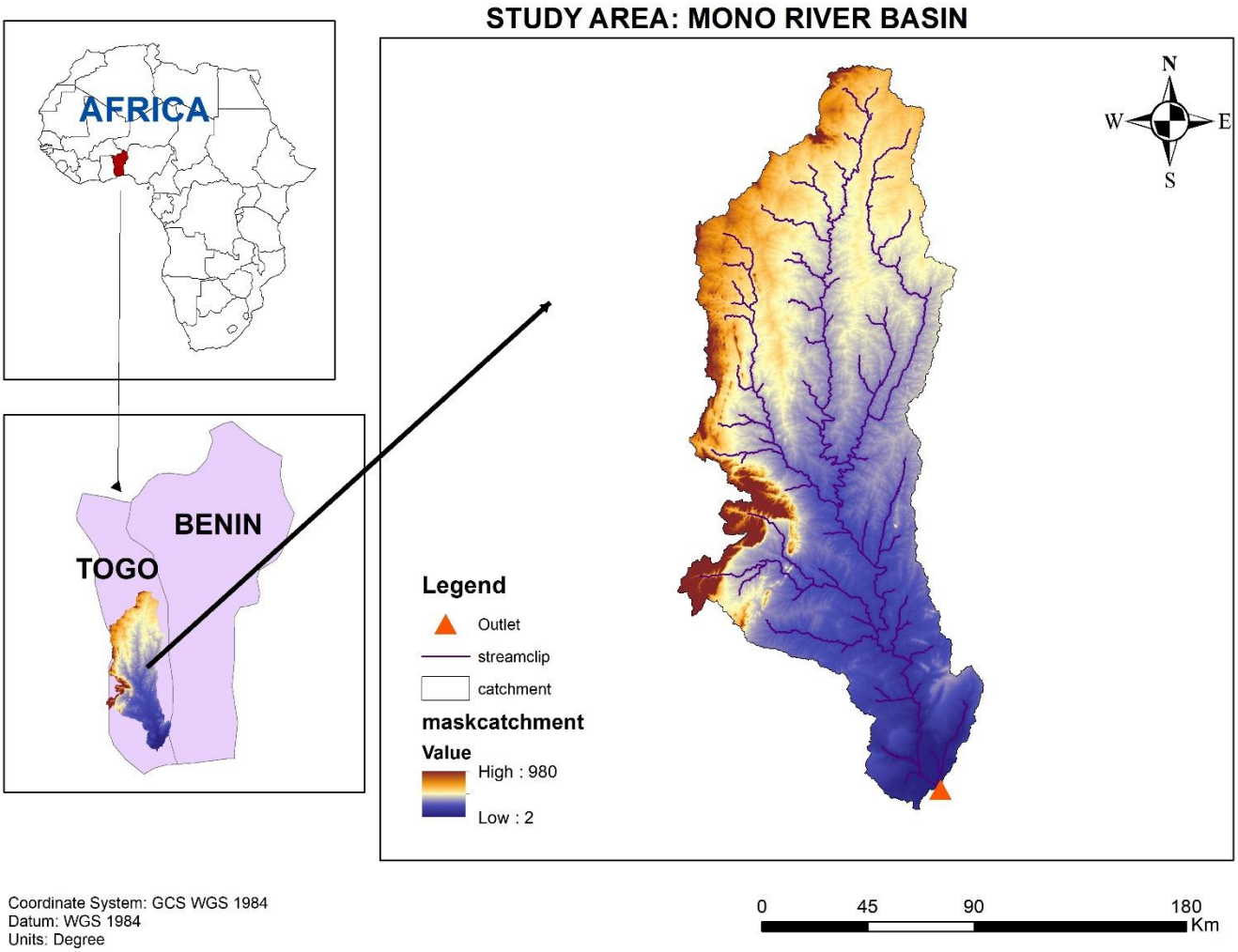

Figure 6. Location of Mono River

A hydroelectric dam called Nangbeto is installed on the Mono River Basin. The study is conducted in the Lower part of the Mono River Basin. As the largest river in Togo, and occupying an area of 23.119 km^2, Mono river extends over 560 km from north to south and more precisely between 06 ° 16 'N and 09 ° 20'N and 0 ° 42 'E and 2 ° 25'E (Amoussou, 2010). It is managed by both Republics of Benin and Togo which have come together to form Mono River Basin Authority for efficient management of water resources over the Basin. The River takes its source water from Atakora table ranges (Mount Togo) at an altitude of about 400 m, the eastern side of the Central region of Togo (Fernando, 2014). Almost every year, people living within the Basin are usually flooded such as Aklakou-Zongo, Avévé, Kpondavé, Adamé, Agbanakin among other villages located in the lower part of Mono River (Ntajal, 2016).

3.2. Population and Economics activities

Agriculture is the main activity carried out in the Mono River Basin with a majority of the people living practicing subsidence farming. This activity is vulnerable to extreme climate events such as drought and flooding.

According to the report of WAEMU in 2006, the populatin of the basin is more than two million, with an annual increase of 2.9%. This population is at high densities in the south of the basin and has rainfed agriculture as main activities ; while those in the lower part, fishing and salt farming are the major activities (Amoussou, 2015; Lamboni et al., 2019).

3.3. Topography, Vegetation, and Soil

The Mono Basin has a coastal sedimentary basin at the south, modeled in littoral plain and plateaus and highest reliefs in the north including the Atacora mountains and their southern extensions, the mountains of Togo.

The lower basin of Mono has a smooth topography due to its partial recovery by sandy-clay alluvium. However, it presents the various levels which undoubtedly mark levels of erosion recovery (Amoussou, 2010). The redistribution of water on the continental surface is highly constrained by geomorphology and surface properties (permeability of soil and subsoil, nature and density of vegetation, etc.). The Basin is formed by hydromorphone soils which are rapidly saturated of water. The sand contents decrease, depending on the closeness of the area to the river. The geology consists of the continental shelf called the terminal plate which extends from Kouvé area to the north-western of Sedome.

The soils in the lower part of Mono River Basin are made up of clay (60%) and sandy clay (40%). Areas which are composed primarily of these types of soils are prone to a higher flood risk because the water requires a longer time to drain or infiltrate into the ground (Ntajal, 2016).

The vegetation is composed of dense forests, savannahs, fallows, crop fields, coconut, grasses and scattered mangoes that rather serve as firewood for some surrounding communities due to increasing demand for fuelwood.

Land use and land cover for the Lower Mono Basin are classified in four groups: Built-up areas/bare soils, coconut and palm plantations, swampy areas, with scattered mangroves (Figure 7). The fauna consists of mammals (buffalo, warthogs, monkeys, deer, agouti, etc.) and various birds of prey, aquatic life, crocodiles and hippos.

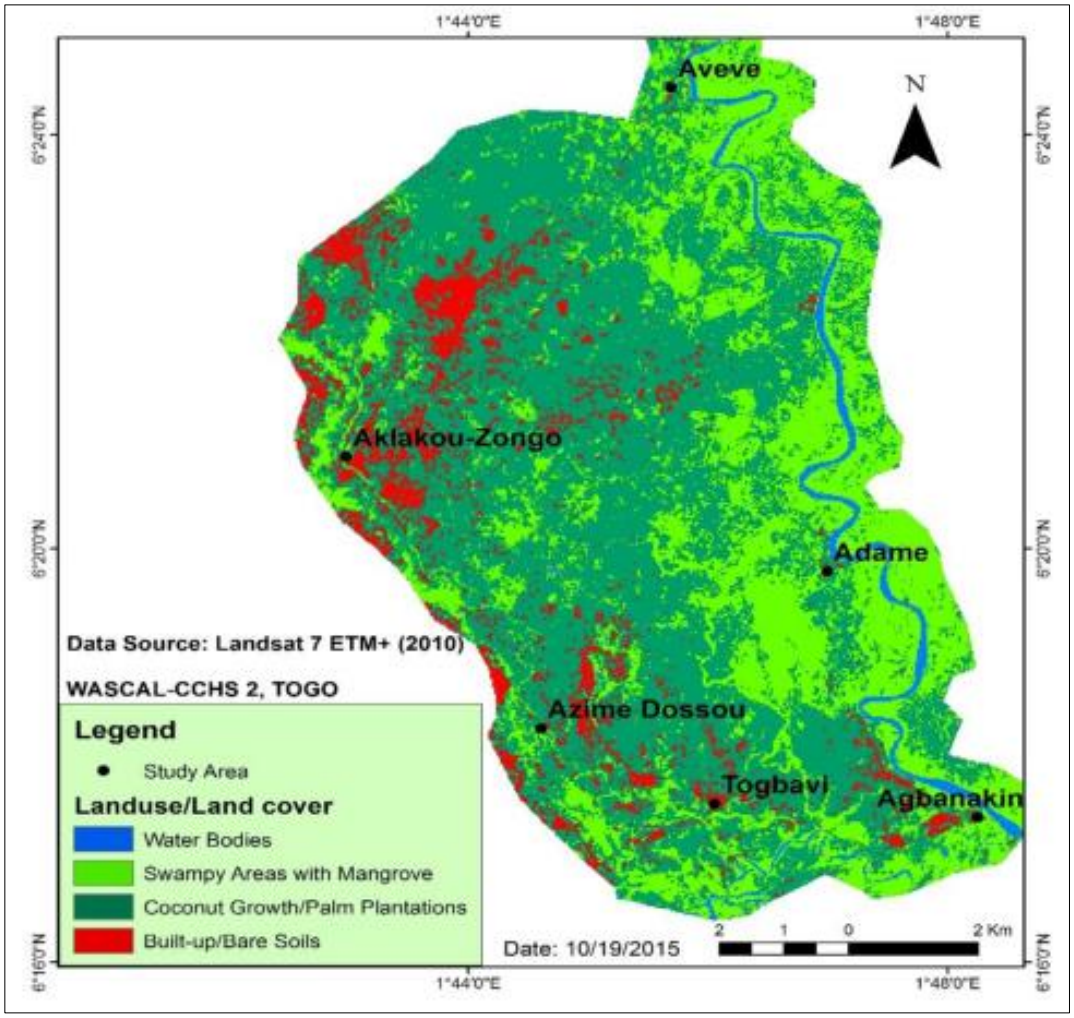

Figure 7. Land use/land cover classification using 2010 Landsat 7 ETM+ image (30 m; Path/Row: 198/52), (Ntajal, 2016)

3.4. Climate

Mono Basin's climate varies from tropical to savanna. It is controlled by the interaction of two air masses; the influence of which varies all over the year with the north-south movement of the Intertropical Convergence Zone (ITCZ). Hot and dry continental air masses originating from the high-pressure system above the Sahara Desert give rise to dusty Harmattan winds throughout most of West Africa from November to February. Moist equatorial air masses originating over the Atlantic Ocean bring annual monsoon rains during summer (Lamboni et al., 2019). The Lower Mono River Basin climate is classified as tropical savannah with a subtropical forest bio-zone. Two types of rainfall regimes are observed in the basin. In the southern basin, (from 6˚16'N to 7˚30'N) there are two rainy seasons which extend from mid-March to mid-July and from mid-August to October. In the northern part of the basin (from 7˚30'N to 9˚20'N), there is one rainy season which extends from April to October (Amoussou, 2010; Ntajal, 2016). The maximum annual rainfall is 1405,47 mm from 1983 to 2010 and the minimum total annual is 840, 56 mm (Figure 8).

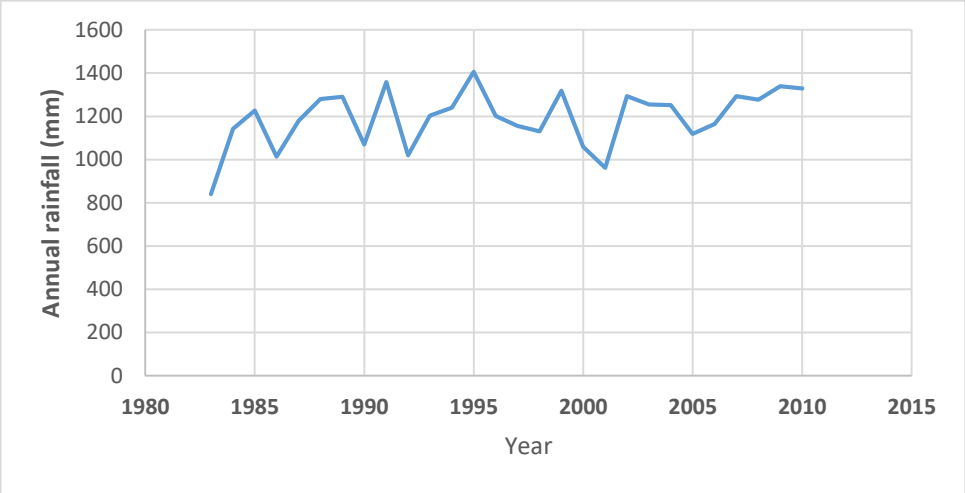

Figure 8. Inter-annual rainfall variability for the period 1983 to 2010

The mean annual maximum temperature is 27.95 °C (2010) for the whole basin while the daily maximum temperature ranges from 22 °C to 32°C between 1983 and 2010, (Figure 9).

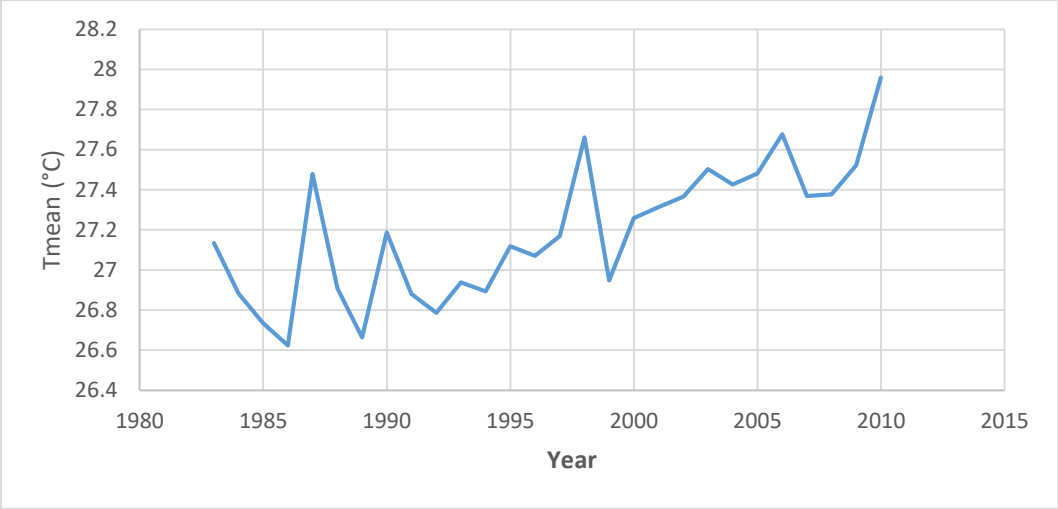

Figure 9. Mean annual temperature for the period 1983 to 2010

CHAPTER FOUR

4. MATERIAL AND METHODS

4.1. Data collection- Data sources

This section provides a description of the data collected. In this study, only secondary data were collected from various sources and used for analysis (Table 2). Secondary data collected are climatic data (rainfall, temperature, relative humidity, solar radiation, and wind speed) and hydrological data (River flow data). These data were collected for the purpose of doing hydrological modeling as input to the HBV model. The DEM (30 m) for the study area was derived from USGS/NASA SRTM data and was in decimal degrees and datum WGS84. The data was downloaded from the CIAT-CSI website (available at http://srtm.csi.cgiar.org).

Table 2. Description of input data

Data type	Description	Source
SRTM (DEM)	Resolution (30 meters)	CGIAR-CSI (http://srtm.csi.cgiar.org).
Rainfall Data (mm)	1983- 2010	National Meteorological Service of BENIN and TOGO (DMN)
Temperature (°C)	1983- 2010	Atakpamè, Bohicon and Savè stations; DMN Togo and Benin
Mono River flow data (m^3/s)	1983 - 2011	Athieme station, Benin General Directorate of Water
Relative Humidity (%), Wind speed (m/s) and Solar radiation (MJ/m^2 .day)	1970 - 2010	Bohicon and Savè stations, Meteorological Service of BENIN
Evapotranspiration (mm/day)	1983- 2010	Atakpamè station; Meteorological Service of TOGO

Daily observed Climatic data were provided by the National Meteorological Service of BENIN and TOGO (DMN, Direction de la Météorologie Nationale) and hydrological data (discharge data) from Benin General Directorate of Water (DGEAU) for the period 1983 to 2010.

Figure 10 shows the hydro-climatic stations where rainfall, temperature, discharge, relative humidity, solar radiation, wind speed data were collected by DGEAU and DMN Benin and Togo.

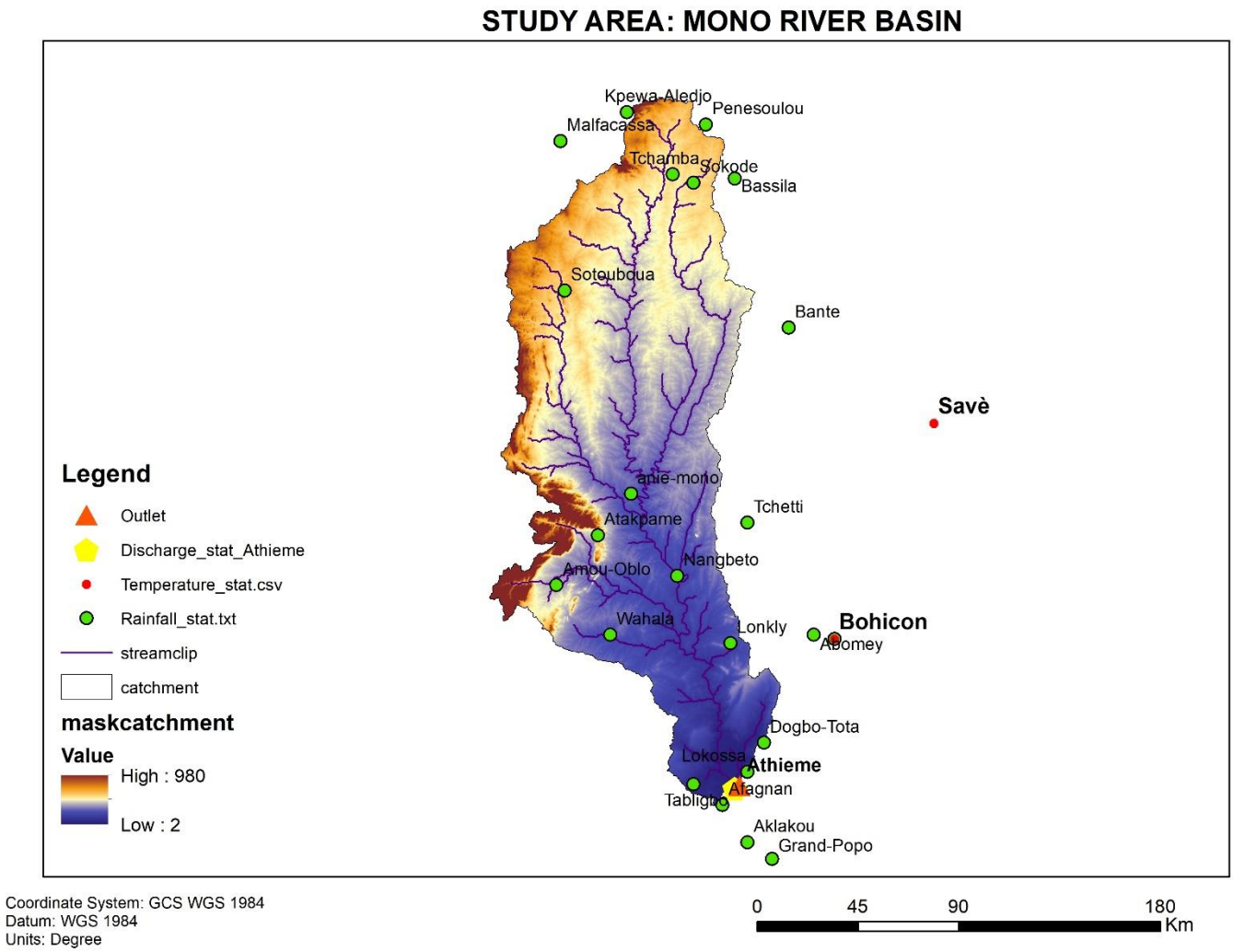

Figure 10. Hydro-climatic stations of Mono Basin

Rainfall data were obtained from 20 rain gauges within and around Mono basin (not farther than 25 km).

Temperature data were collected from three synoptic stations within the basin (Taligbo, Atakpamé, and Sokodé) and two other stations near the basin (Bohicon, Savè).

Relative humidity, Solar radiation and Wind speed were collected from two stations, Savè and Bohicon, near Mono basin for the period. These data were used to compute potential evapotranspiration at Savè and Bohicon stations using Eto Calculator. As for Atakpamè station, Evapotranspiration data was available at the Meteorological Service of TOGO.

4.2. Hydrological modeling

The availability of hydrological and climatic data promotes confidence in the hydrological modeling effort (Miller et al., 2012). Different types of data also make it possible to constrain the uncertainties in the predicted variables (Pappenberger et al., 2006), leading to more accurate model results.The hydrological model selected for this study is the HBV model. The data required to set up the HBV model are: areal precipitation, temperature, discharge and evapotranspiration.

4.2.1. Data Processing for HBV Simulation

This section explains the methods used for data processing. To calibrate and validate the model, there is a need for analyzing the collected set of data such as climatic data and Hydrological data.

4.2.1.1. Processing of Rainfall data

First of all, visual interpretation was done. This showed the data format and the way they were arranged for the 20 rainfall stations. The missing data were filled using data from the nearest stations. Microsoft office excel and R software were used to process rainfall data. R software was used to transform them into two columns, one for the years and the second for rainfall data. After transforming all stations data with R Software, there were combined in one table . Areal precipitation was then computed to prepare the PTQ file.

- **Areal Precipitation computation**

The rainfall is never the same over the entire basin but it varies spatially in intensity and duration. In order to be used in the HBV model, rainfall data for all stations were considered and spatial interpolation was done. This study considered Thiessen polygon and Kriging Ordinary methods. However, the output from kriging was used for HBV-light model set up as the one from thiessen polygon method was not suitable.

- **Thiessen polygon method** (weighted mean method)

Different steps were undertaken to develop the Thiessen polygon for the study area. Arc Gis spatial analyst tool was applied to computed the weighted coefficient. Firstly, rainfall stations were projected in the study area already delineated). By selecting “Analysis Tools, Proximity and Create Thiessen Polygon”, in Arc Toolbox, rain gauge’s locations were joined so as to form a network of

triangles. Then perpendicular bisectors were drawn to the triangle sides. Thus, these bisectors formed polygons around the stations.The following formula was applied to compute the weighted coefficient for each station:

$$C_i = \frac{Ai}{AT} \quad \textbf{(15)}$$

Where C_i is the weighted coefficient for each station, A_i the area of the corresponding polygon and AT the total area of the basin. The rainfall recorded at each station was weighted according to the area, it represents. To compute the areal precipitation, the following equation was applied:

$$P_i = C_i * R_i \quad \textbf{(16)}$$

where P_i is the weighted precipitation, C_i the weighted coefficient, and R_i the rainfall recorded at the ith station.To get daily areal precipitation for the basin, the following formula was applied:

$$P_{areal} = \sum_{i=1}^{20} Pi \quad \textbf{(17)}$$

where P_{areal} is the Areal daily areal precipitation of our basin.

- **Kriging interpolation method**

The Kriging method presented a suitable result which was then applied to run the model. This also confirmed the work done by (Amoussou, 2015; Houngue, 2018), who applied the same method in the same basin.

4.2.1.2. Temperature data processing

There were no missing values in temperature data collected at the three stations (Taligbo, Atakpame, and Sokode) located within Mono basin as well as at Bohicon and Savè stations.

The arithmetic mean of the five stations was used by applying the following formula:

$$T_{mean} = \frac{\sum_{i=1}^{5} Ti}{n=5} \quad \textbf{(18)}$$

where T_{mean} is the average daily temperature in Mono Basin, Ti the temperature recorded at the ith station and n the number of stations (n = 5, for the 5 stations used to compute our Tmean).

4.2.1.3. Processing of River Flow Data

Daily discharge data were required in the calibration processes to simulate discharge at the outlet of the basin and adjust the model parameters.

First of all, a visual interpretation of Athieme discharge was done. It has been found that the discharge data contains numerous missing data. Using the Pivot table in Microsoft Excel office,

the percentage of missing data per year was determined. Especially, for the years 1995 and 2001 observation data was not available.

Only for the years 1988, 1989, 2009 and 2010, there were no missing data. As for, the years 1985, 1990, 1991,1992, 1997, 1998 and 2000, the percentage of missing data was less than 20% while it was less than 60% for the years 1986 and 1987. These years could also be considered for hydrological modeling.

4.2.1.4. PTQ file

After processing rainfall (P), temperature (T) and discharge (Q) data, Microsoft office excel was used to put each variable in one column and the years (1983-2010) in another one. The discharge data were replaced by "-99". The PTQ file was saved in Text Document (.txt) files.

- **Evapotranspiration, ETo, (Evap) file**

Evapotranspiration at Savè and Bohicon stations was determined using ETo calculator software, version 3.2 (FAO, 2012). For Atakpame station, Evapotranspiration data (ETo_1) was available at the meteorological institute of Togo. It was computed using Hargreave – Samani's formula (Hargreaves & Samani, 1982). To compute evapotranspiration for Bohicon and Savè stations as well as for the study area, missing data contained in relative humidity, solar radiation, and Wind speed were firstly filled using the mean arithmetic method for each station. For the missing days in a month, gaps were replaced by the average of days for that particular month. As for a missing month in a year, the gap was filled by the average of that month in the time series.

The mean of Temperature, Relative humidity, Solar radiation, and Wind speed for the two stations were computed and used as an input data in ETo calculator to get mean evapotranspiration (ETo_2). The mean arithmetic of Atakpame's evapotranspiration, ETo_1, and the one obtained from the ETo Calculator, ETo_2, were considered as the evapotranspiration of Mono basin (ETo). The Evap file was thus created.

4.2.2. HBV model set-up

Model calibration is a systematic process of adjusting the model parameter values in order to obtain the best fit between the observed data and simulated results as well as to get the reality within the range of accuracy defined by the efficiency criteria (Manyifika, 2015). Following the input data required by HBV-light model (2.1.3.1. Data requirement), PTQ (Rainfall, Temperature, and Discharge) and Evapotranspiration data were used in calibration and validation of the model. Firstly, the available data time series (1983-2010) were considered to run HBV-model in order to

identify years where the simulated hydrograph match well with the observed one. Those years (1986- 1992; 1985 and 2010) were then chosen for the calibration and validation periods. The period,1986 -1992 was split into calibration (1986 – 1990), and validation (1991 -1992) periods. The years 1985 and 2010 were also used for validation of the model. Besides, 1986-1990 (5 years) is only the large range of years which contains less missing discharge data (less than 20%) as well as years (1985, 1988, 1989,1990, 1991, 1992 and 2010) without missing data during rainy season (April – November). It also accounts for high discharge years, 1988,1989 and 1990 (Houngue, 2018).

During the calibration process, the model was initially run 10. 000, 50.000 and 70.000 times with broader parameter ranges to identify suitable parameter bounds for Mono basin. Afterward, 70,000 model runs within these parameter bounds were used to derive behavioral parameter data.

The parameter sets were treated as being behavioral in calibration and validation periods according to three goodness-of-fit criteria: The Nash Sutcliff efficiency (NSE), Coefficient of determination R^2 and Kling- Gupta (see 2.1.3.2. Calibration and 2.1.3.4. Performance evaluation of the model) with needs to be ≥ 0.50 to consider the model efficient in simulating discharge. The same objective functions have been applied in other studies (Booij, 2005; M G Grillakis et al., 2010; Houngue, 2018).

The principle consisted of varying the parameters till a relatively good efficiency coefficient is obtained for the calibration period. These parameters were then used for validation periods. The hydrograph produced by the observed streamflow data and the one simulated were also compared to see if there are closed. In fact, HBV-light was automatically calibrated using the Genetic calibration algorithm GAP embedded in the model.

4.3. Evaluating climate change impact on water balance components

Climate change impact on hydrological processes depends on the projected future climate scenarios provided by climate models (Maghsood, Reza, Bavani, Panahi, & Berndtsson, 2019).

4.3.1. Data sources

Daily climatic data (Precipitation, Temperature minimal and maximal, relative humidity and Wind speed) were provided by two models (the Global Circulation model GFDL-ESM2M and HadGEM2-ES) under the Representative Concentration Pathway RCP 4.5 downscaled by Wascal

(Heinzeller et al., 2018) for the historical period 1980-2005 and two future periods (2020-2049 and 2070-2099).

4.3.2. Data processing and evaluation

To process and evaluate the output from GFDL-ESM2M and HadGEM2-ES models, the following procedure were used:

Firstly, the simulated data by GFDL-ESM2M and HadGEM2-ES were processed using Microsoft excel software (Pivot table). The missing data were identified and gaps were filled in each data series using arithmetic mean method. Daily average temperature were computed using daily maximal and minimum temperature; then potential evapotranspiration were calculated with Eto calculator software version 3.2 for the simulated historical and future periods.The historical period were defined taking into account the time series of the observed (1983- 2005) and model simulations data (1980-2005). Historical observed data (precipitation and temperature) were plot against model simulations to analyze the gap between both. This helps to verify the existence of bias.

Secondly, in this study, the output (precipitation and temperature) from GFDL-ESM2M and HadGEM2-ES as well as computed potential evapotranspiration (Eto) was bias corrected using quantile mapping method (see 2.2.4). Quantile mapping code were written in R software for the bias correction. The calibration period were chosen based on the reference period (1983-2005). The transfer function (coefficient of correction) generated between the historical observed and simulated data were applied to the projected future data (2020-2049 and 2070-2099) for correction. Bias correction data were evaluated by comparing corrected and uncorrected precipitation, temperature and potential evapotranspiration (Eto) respectively.

4.3.3. Future projected discharge simulation and climate change signal analysis

Future discharge were firstly simulated using uncorrected and corrected climate data to obtain bias uncorrected and corrected discharge respectively. The trends in precipitation, temperature, Actual Evaporation and discharge were then analyzed with the bias corrected and uncorrected values in order to also assess the effect of the application of quantile mapping method on the climate trend in Mono basin.Climate change signal were determined by plotting data for the three range of years (1983-2005; 2020-2049 and 2070-2099) with the reference, historical period (1983-2005). The change signal were calculated using the following equation:

$$\% \text{ Change} = \frac{Fi - Hi}{Hi} * 100 \quad (19)$$

where Fi is the future variable and Hi, historical variable.

4.4. Flood frequency analysis and detection of change due to climate change

The analysis of the climate change impact on flood frequency represents an important issue for water resources management and flood risk mitigation. In frame of the present study, flood frequency was based on annual maxima discharges for the historical period (1983-2005) and future periods (2020-2049; 2070-2099) under the assumption that there are no changes in the features of the basin. The frequency analysis was applied to discharges from GFDL-ESM2M and HadGEM2-ES models.To achieve the frequency analysis, the following procedure were adopted.

Annual maxima discharge were firstly extracted from the bias corrected discharge series. Then, four different distributions (Generalized Extreme Values, Weibull, Gumbel and Pearson type III) were fitted to the maximum annual discharges from each of three periods , and parameters of these distributions were estimated using the method of maximum likelihood and the methods of moments. Calculations were performed with HYFRAN Software version 1.1 (Salaheddine & Bobée, 2015). The procedure consisted of computing for each probability distribution and for the same parameter estimation method (if available), the flood quantile (XT), the probability of non-exceedance (q) and the corresponding return period (T) for the historical and two future periods.

For each times series, a comparison was done between the four probability distribution results, based on two models selection criteria: the Bayesian Information criterion (BIC) and Akaike Information Criterion (AIC), (Ehsanzadeh et al., 2010). The best fit probability distribution was thus identified. The probability distribution recording the lower BIC and AIC was considered as the best fitting the discharge series (Giuliano et al., 2009). Therefore, its results were used to calculate the percentage change of the future quantiles based on the historical quantiles. Hence, percentage change showed the impact of climate change on flood frequency in the Mono Lower basin.

CHAPTER FIVE

5. RESULTS AND DISCUSSION

This chapter presents the results obtained from hydrological modeling, climate change signal and impact assessment on the flood frequency for historical and future periods for the study area.

5.1. HBV model set-up

This section explains the results obtained from calibration and validation of HBV model.

5.1.1. Calibration

Calibration of the model is a process of setting model parameters so that the simulated results match with the observed data and it is done after making a comparison between the simulated and observed discharge results. After running the HBV model with different sets of parameters, the parameters giving the best fit between the observed and simulated discharges are presented in Table 3.

Table 3. Calibration parameters

Calibration parameters	Values	Calibration parameters	Values
Alpha	0	CFMAX	3.516
K0	0.311	CFR	31.843
K1	0.212	CWH	0.931
K2	0.073	FC	1116.729
MAXBAS	6.773	LP	0.693
PERC	2.282	SFCF	1.467
UZL	33.759	SP	0.141
BETA	3.224	TT	23.316

Based on the observed rainfall, temperature, and evapotranspiration data for the period 1986 to 1990 (5 years), the hydrograph simulated by HBV model as shown in Figure 11, was obtained at

the outlet (Athieme) of Mono basin. It shows a strong correlation between observed and simulated discharges.

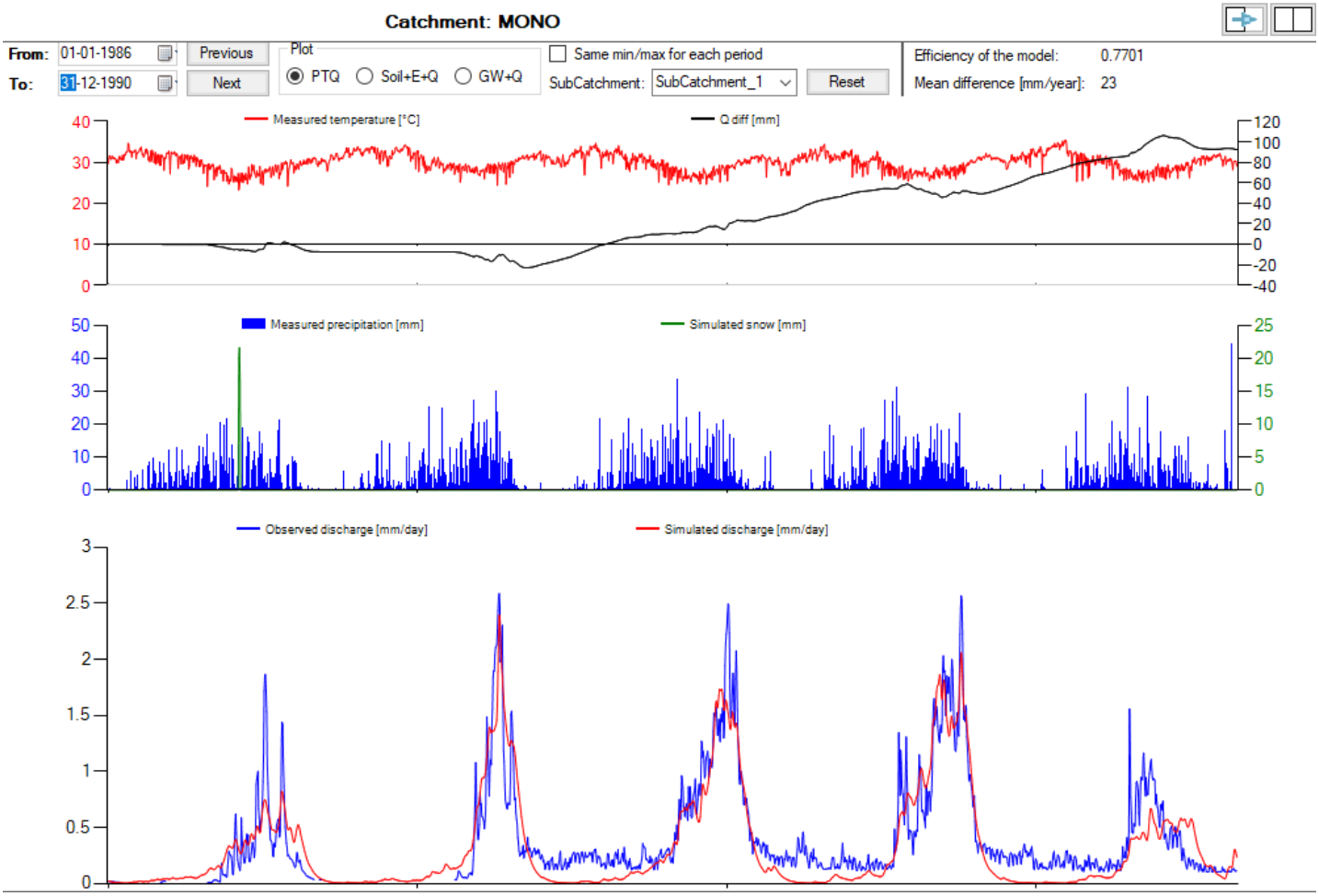

Figure 11. Observed and simulated Hydrographs for the calibration period 1986 -1990

Satisfactory results are obtained as shown by Table 4, where the objective function, Nash- Sutcliff Efficiency coefficient (NSE) is relatively high reaching the value of 0.77. In addition coefficient of determination is 0.794 and Kling-Gupta efficiency is 0.820. These performance results are above the normal reference 0.50 (see 4.2.2. HBV model and shows that HBV model can significantly well simulate the discharge in Mono Lower basin over the calibration period 1986 to 1990.

Table 4. HBV model efficiency results for the calibration period

Goodness of fit	**Calibration results**
Model efficiency (Nash-Sutcliffe E)	0.770
Coefficient of determination (R^2)	0.794
Kling-Gupta efficiency	0.820

5.1.2. Model Validation

Following the satisfactory calibration results, the HBV-light hydrological model was validated with the calibration parameters. As mentioned in section 4.2.2. HBV model , three independent periods (1991- 1992; 1985 and 2010) were used to validate the model.

Validation also shows satisfactory results (Table 5); according to the goodness of fit criteria for the validation periods 1991-1992 and 2010 where NSE, R^2 and KGE are greater than 0.80. As for the model validation in year 1985, NSE and R^2 = 0.551 while KGE =0387<0.5 (normal reference). Although, KGE is below 0.50 for the validation in year 1985; the objective function, NSE and the coefficient of determination, R^2 are above 0.5. However, these values are lower compare to those obtained during validation over period the 1991-1992 and in 2010. Therefore, a better match between the observed and simulated discharges was found for the period 1991- 1992 and 2010 compared to 1985. Figure 12, Figure 13, Figure 14 also confirm these results by showing a low underestimation in simulated discharge in year 2010 compared to 1985.

Table 5. HBV model efficiency results during validation periods

Goodness of fit	**Validation results in 1985**	**Validation results on period 1991-1992**	**Validation results in 2010**
Model efficiency (Nash-Sutcliffe E)	0.551	0.819	0.813
Coefficient of determination (R^2)	0.551	0.820	0.883
Kling-Gupta efficiency (KGE)	0.387	0.883	0.650

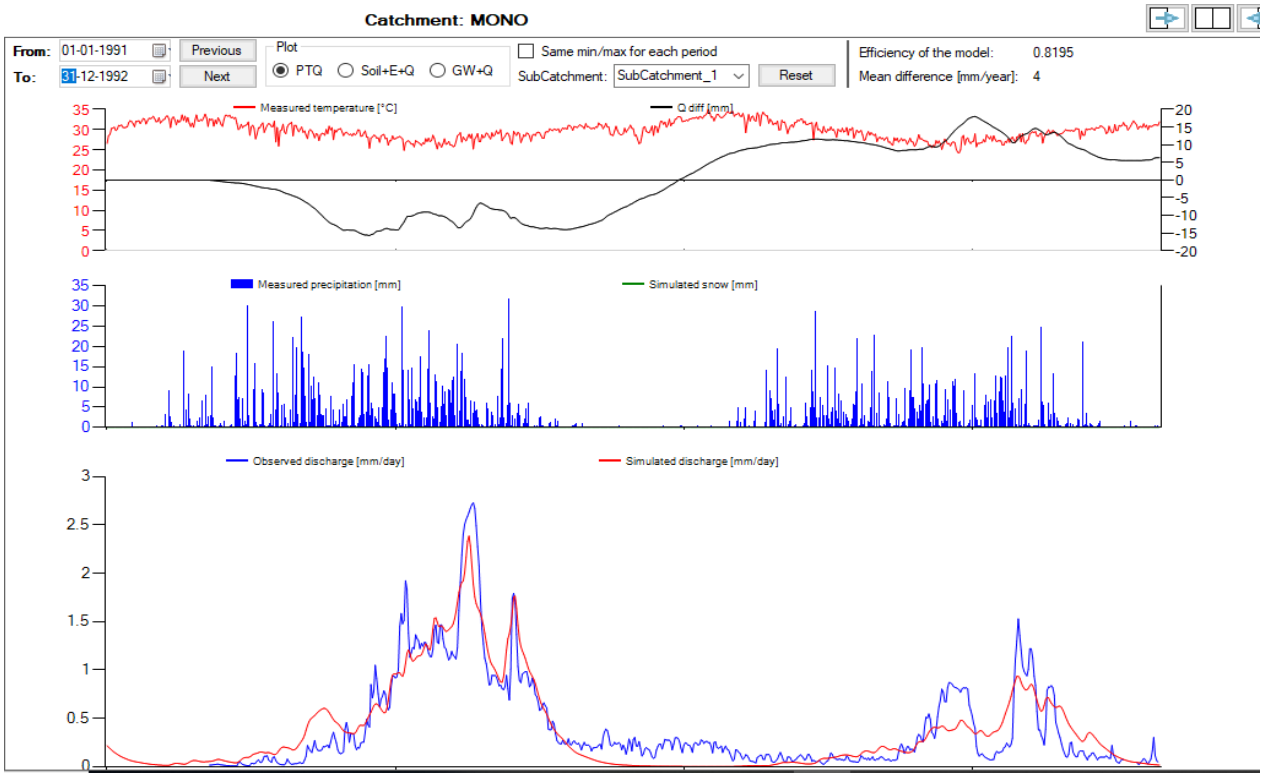

Figure 12. HBV model validation for the period 1991-1992

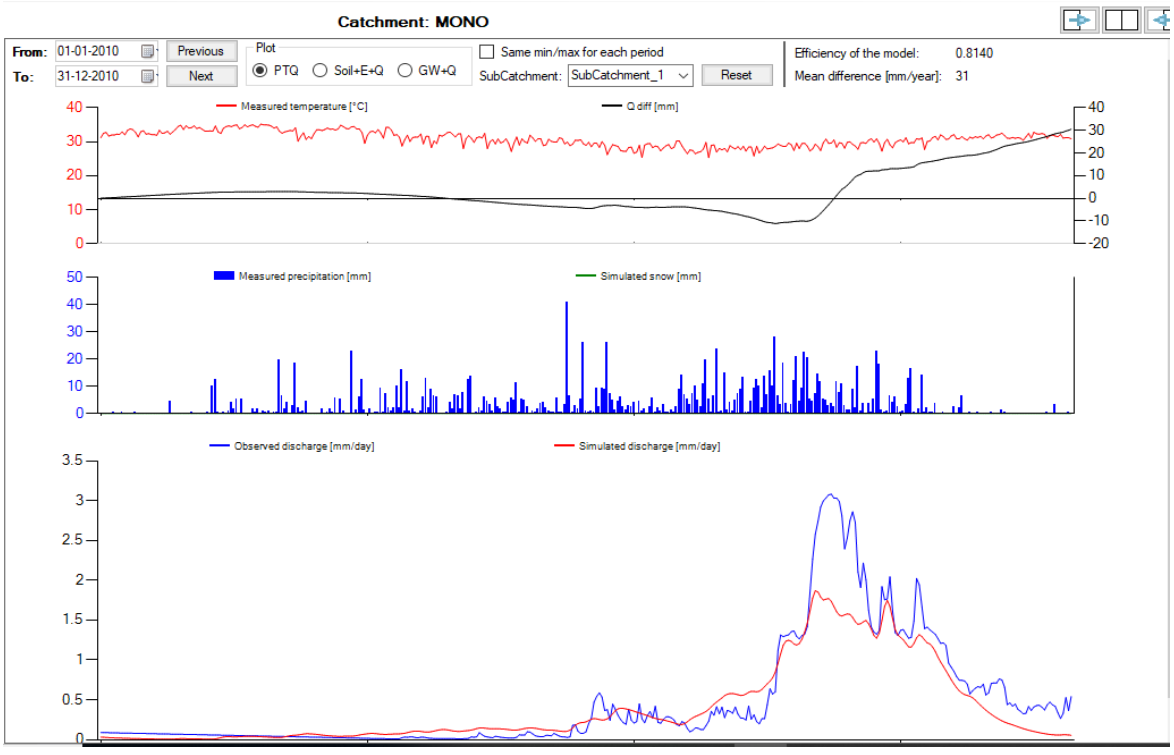

Figure 13. HBV model validation in year 2010

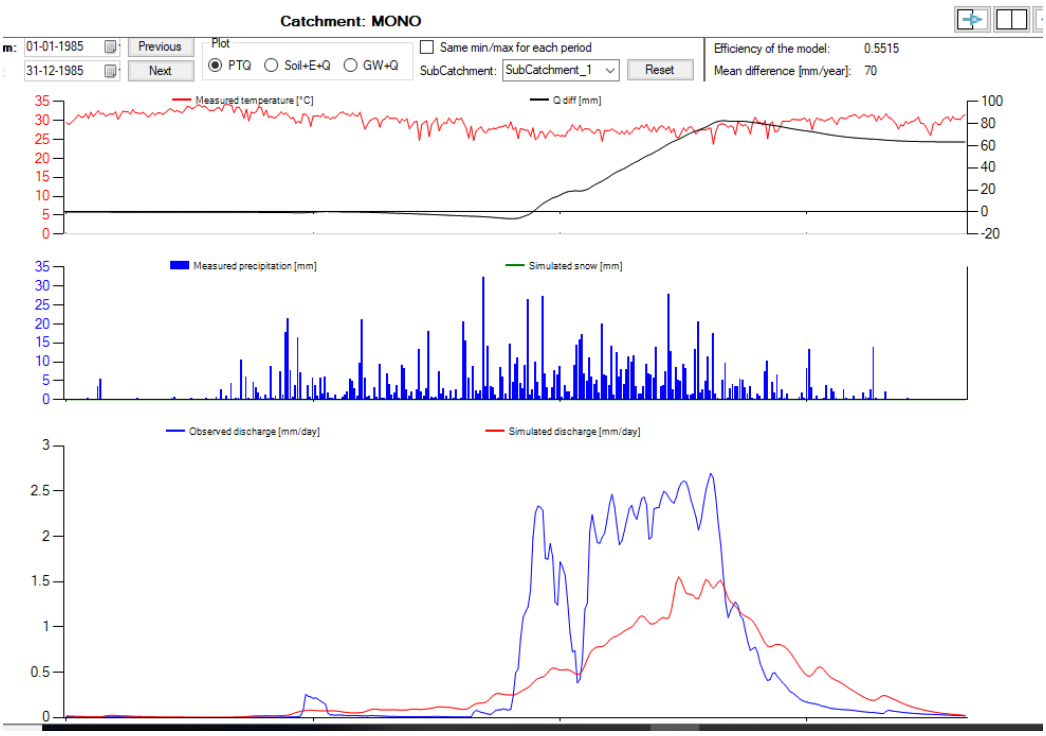

Figure 14. HBV model validation in year 1985

Overall, the simulation of discharge using HBV-light provided encouraging results. The model shows well performances in view of the NSE and R^2 >0.5 thus testifying a good ability to reproduce the discharge of the Mono basin.

5.2. Discharge analysis

Simulated discharge over the study period 1983- 2010 is presented in figure 15**.** Over that period, the range of annual maximum discharge at the outlet of the Mono basin is between 178 m^3/s and 640.6 m^3/s. The highest value was recorded in 1987 while the lowest in 1990.

Figure 15 shows that the variation of annual maximum discharge match well with annual rainfall over the period 1983 to 2010. Hence a decrease in discharge occurs when the rainfall decreases and an increase in discharge occurs when rainfall also increases except for the period 1983-1985 and 2008-2008 which could be due to uncertainties in the model simulation.

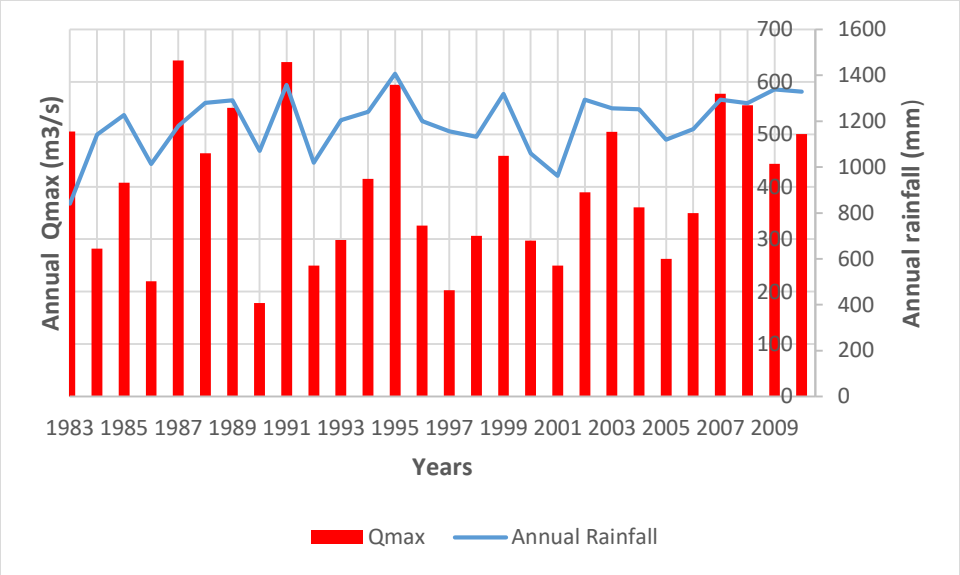

Figure 15. Trend of annual maximum discharge (Qmax) and annual rainfall in Mono basin

The mean monthly hydrograph (Figure 16), reveals there is an increase in discharge from June (56.08 m^3 /s) to October 256.40 m^3 /s, with peaks flow in September (283.70 m^3 /s) and October. The minimum discharge is 3.83 m^3 /s.

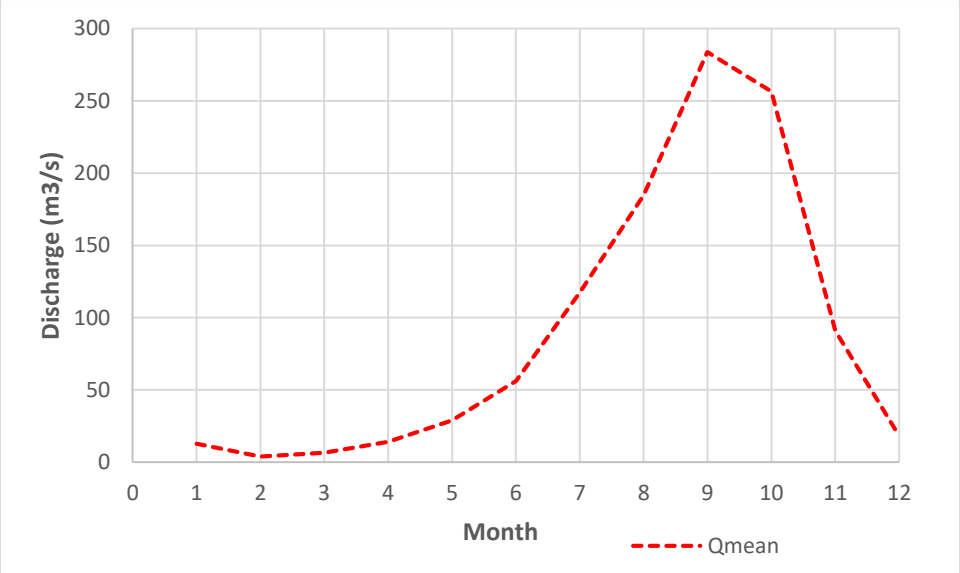

Figure 16. Mean Monthly hydrograph of Mono River

5.3. Climate models' outputs analysis

5.3.1.Uncorrected climate model outputs

The simulated climate data (rainfall and temperature) for the period 1983 to 2005, provided by the climate model HAGEM2 and GFDLESM were compared to the observed data for the same period (figure 17) . Figure 17 reveals that there is a difference between the observed and simulated climate data (rainfall and temperature) for both models.

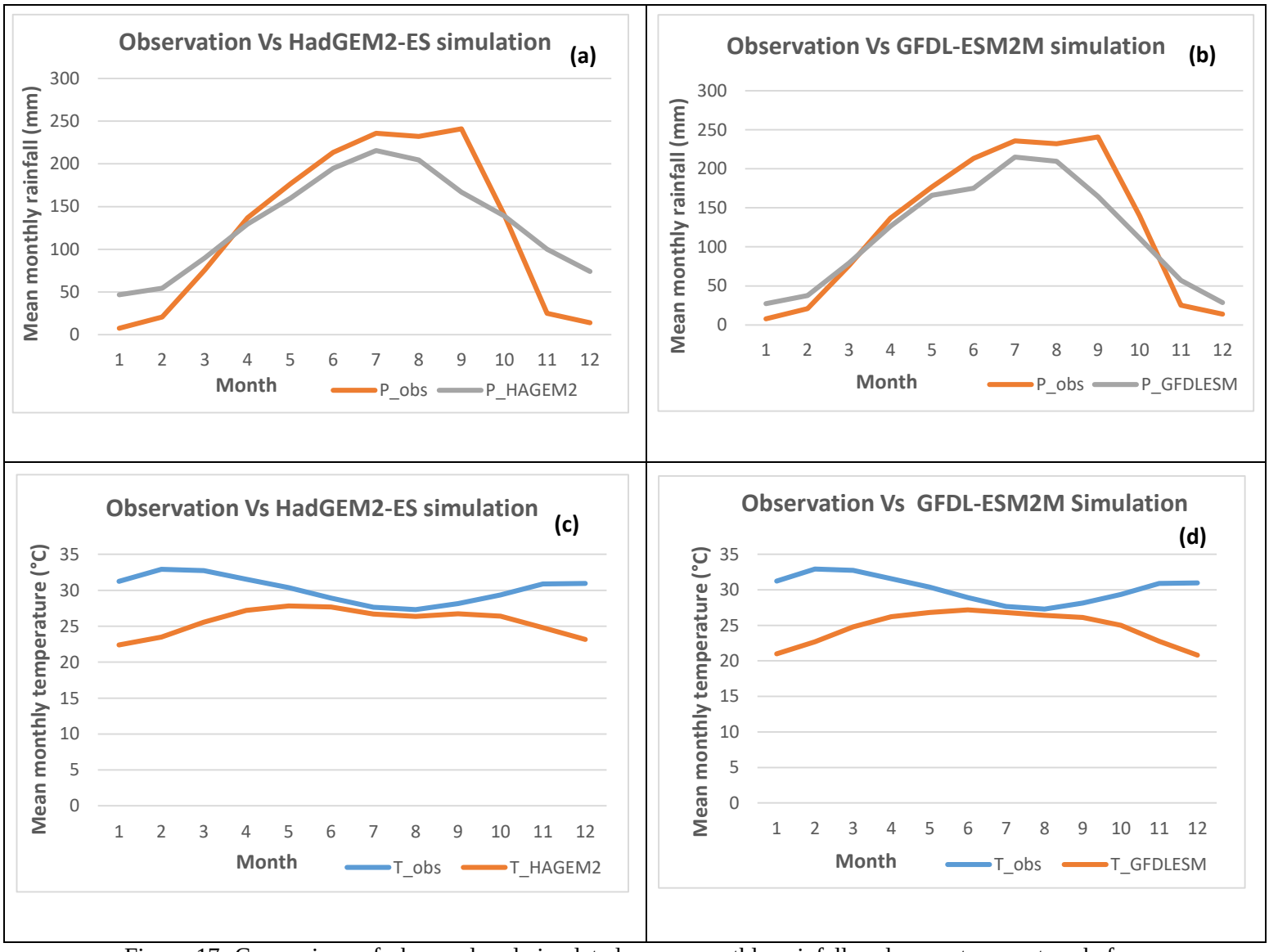

Figure 17. Comparison of observed and simulated mean monthly rainfall and mean temperature before correction over the period 1983-2005; (a) and (c)- HadGEM2-ES simulation; (b) and (d)- GFDL-ESM2M simulation

It is therefore important, to reduce the biases in climate data before analyzing the: projected climate in the basin.

5.3.2. Projected climate data correction using the quantile mapping

Projected raw climate data (rainfall, mean temperature and computed potential evapotranspiration Eto) from two regional climate model, GFDL-ESM2M and HadGEM2-ES under the Representative Concentration Pathway (RCP 4.5) were corrected using Quantile mapping method. The bias corrected data by the above mentioned two regional climate models were compared to the uncorrected data. Figure 18, Figure 19 and Figure 20 present the resulting plots before and after applying quantile mapping.

As illustrated by the first graphs (c, d,g, h) in Figure 18, Figure 19 and Figure 20, the gap between the observed and simulated data (precipitation, temperature) is expressed by the mean distance between the bisector of the central plot and the Transfer function (TF). The transfer function is generated between the simulated and observed data. Therefore, the rightmost bias corrected graphs shown that observed and simulated data are all adjust on the bisector of the central plot. An early conclunding remark about it, is that the bias in simulated data are minimized, hence observed and simulated models data are statistically closer.

Futhermore, after applying quantile mapping method Figure 20, a, b, e,f , i, and j), the Cumulative Distribution Function (CDF) curves of the, simulated corrected data, (green line) overlapped the observed data (black line).This removed the gap between the simulated data (HadGEM2-ES and GFDL-ESMSM models) and the observed data by Transfer Function (TF). The transfer function generated between the observed and simulated data for the reference period (1983-2005) is then used to adjust bias of 30- year moving window from 1983 -2005 to 2020-2049 and 2070-2099. As result of the application of bias correction in this study, the difference between the CDF of the climate models outputs and that of the observations are minimized.

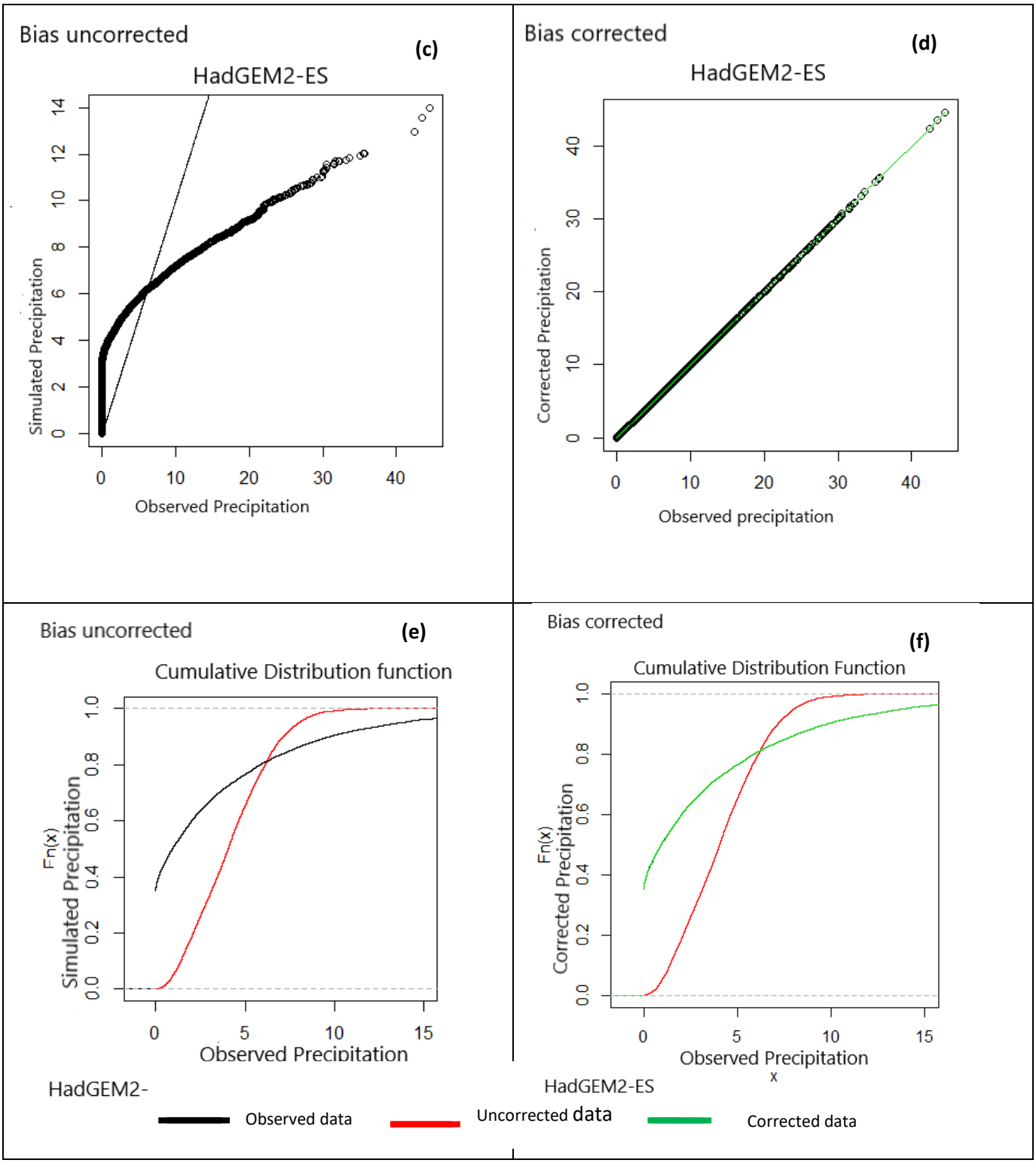

Figure 18.Uncorrected and bias corrected historical rainfall (HadGEM2-ES); (c) and (e)- uncorrected; (d) and (f)- bias corrected

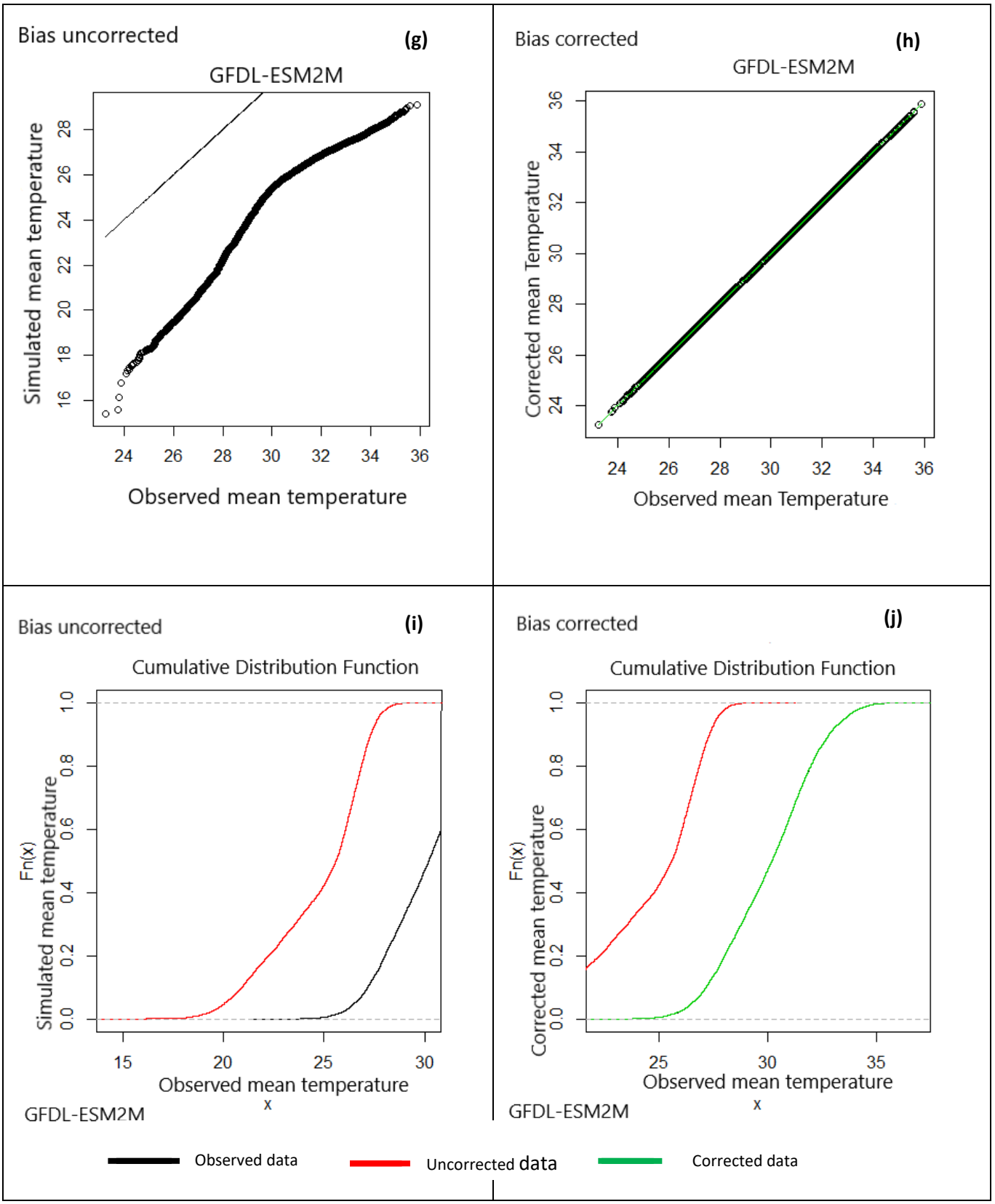

Figure 19.Uncorrected and bias corrected historical temperature (GFDL- ESM2M); (g) and (i)- uncorrected; (h) and (j)- bias corrected

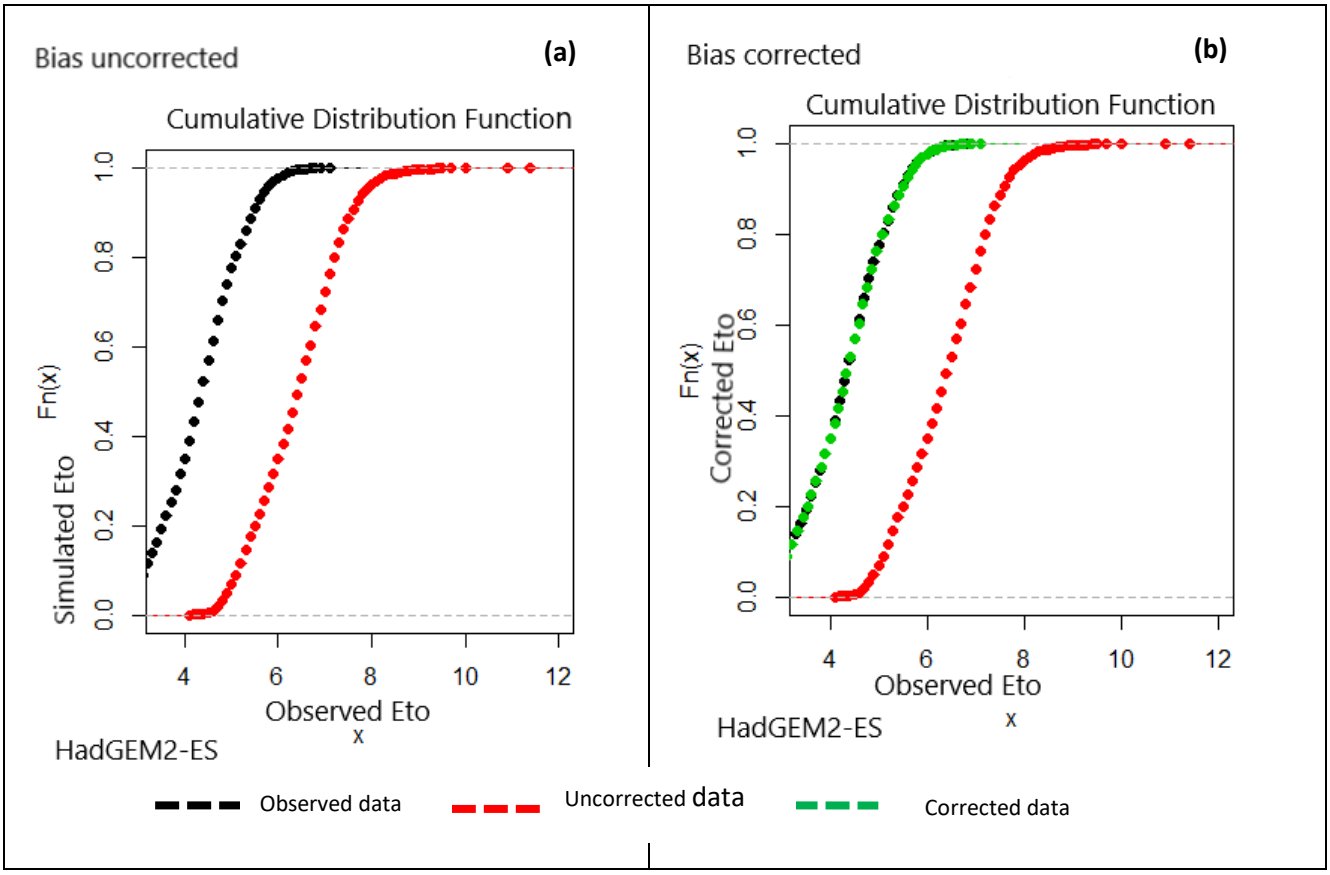

Figure 20.Uncorrected and bias corrected historical Evapotranspiration, Eto (HadGEM2-ES), (a)- uncorrected and (b)- bias corrected

5.4. Climate change Signal (HadGEM2-ES and GFDL-ESM2M) on water balance components

The change signal in climate and hydrological variables (precipitation, temperature, and discharge) expresses the difference between projected and historical values. In this study, both uncorrected and bias corrected (precipitation, temperature, evapotranspiration and discharge) are considered for the trend analysis. While the trend in precipitation (Figure 21, a, b) are the same before and after bias correction, increase in future precipitation from august to december compared to the historical period (1983-2005), there is an increase in the maximum monthly bias corrected precipitation (302, 351, 414 mm) compared to uncorrected precipitation (215, 224, 238 mm) during the rainy season, from July to September, where the peak flow is observed. The same trend is observed with temperature **(**Figure 21, c, d) where the mean maximum monthly bias corrected

temperature (32.71; 33.74; 35.67) are higher than uncorrected values (27.81; 29.45; 30.76) for respectively periods 1983-2005; 2020-2049 and 2070-2099.

Figure 21, also shows an increase in future temperature relative to 1983-2005.

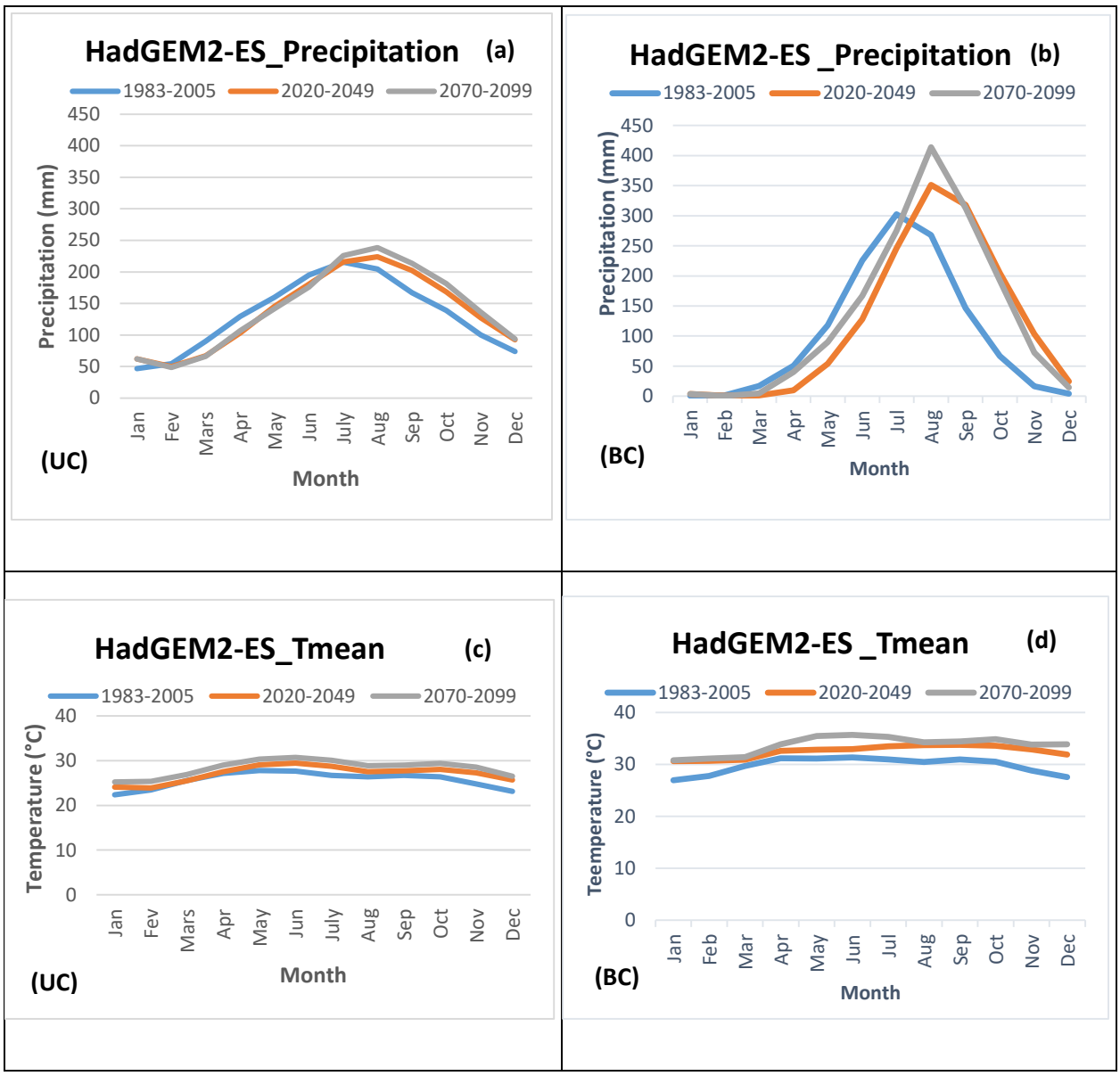

Figure 21. Climate change signal of precipitation and Temperature (Tmean), between the reference (1983-2005) and future (2020-2049 and 2070-2099) periods under emission scenario RCP 4.5. (a) and (c)- uncorrected; (b) and (d)- bias corrected. BC is bias corrected and UC refers to uncorrected bias (HadGEM2-ES)

As for the Actual Evapotranspiration (AET), (Figure 22, a b), there will be an increase in future evapotranspiration compare to the past. Maximum monthly bias corrected AET (113.8;

121.1; 131.9) are smaller than uncorrected AET (149.41; 153.2; 159.4) respectively for the periods 1983-2005; 2020-2049 and 2070-2099.

Figure 22 (c, d) depicts an increase in future discharges (2020-2049 and 2070-2099) compared to historical period (1983-2005). Discharges by 2100 are higher than those of the middle of 21st century. Except the months November and December where precipitation by 2100 is low compared to 2050 while Actual evapotranspiration is higher. The same trend observed for precipitation and temperature is observed for the discharge bias corrected and uncorrected. In one hand, for both historical and future periods, Figure 21 .b and 22.b- d show that low discharge are observed from january to March and in december when there is less rainfall and high evapotranspiration. In another hand, higher discharge are observed during the main rainy season from June to October when the maximum rainfall induced peak flow in September.

HadGEM2-ES projects an increase in climate and hydrological variables of about 19% for precipitation, 9% for AET and 59% for Discharge by 2050, whereas 35% for precipitation, 20% for AET and 102 % for discharge by 2100 (Table 6). However, there is a decrease in future discharges from June to July due to the decrease in future precipitations from February to July and the increase in future Actual Evapotranspiration relative to the baseline (1983-2005). As for temperature, it will increase from 0 to 1.17°C in the first future period and from 1.17°C to 3.20°C in the second future period. This change in climate signal is relative to the reference period (1983-2005). The change in discharge signal highlights that high discharge will be recorded in future Mono basin will be more flooded compared to the past if nothing is done.

Table 6. Projected climate variables change between the reference (1983-2005) and future (2020-2049; 2070-2099) with bias corrected and bias uncorrected HadGEM2-ES simulations

HadGEM2-ES	**Uncorrected**			**Bias corrected**		
Period	Historical (1983-2005)	Change (2020-2049)	Change (2070-2099)	Historical (1983-2005)	Change (2020-2049)	Change (2070-2099)
Precipitation (mm)	1576	4%	7.0%	1216.8	19%	35%
Temperature (°C)	25.69	1.63°C	2.65°C	30.1	1.17°C	3.20°C
AET (mm)	557	3%	6%	1008.3	9%	20%
Discharge (mm/day)	136.52	11%	15%	218.3	59%	102%

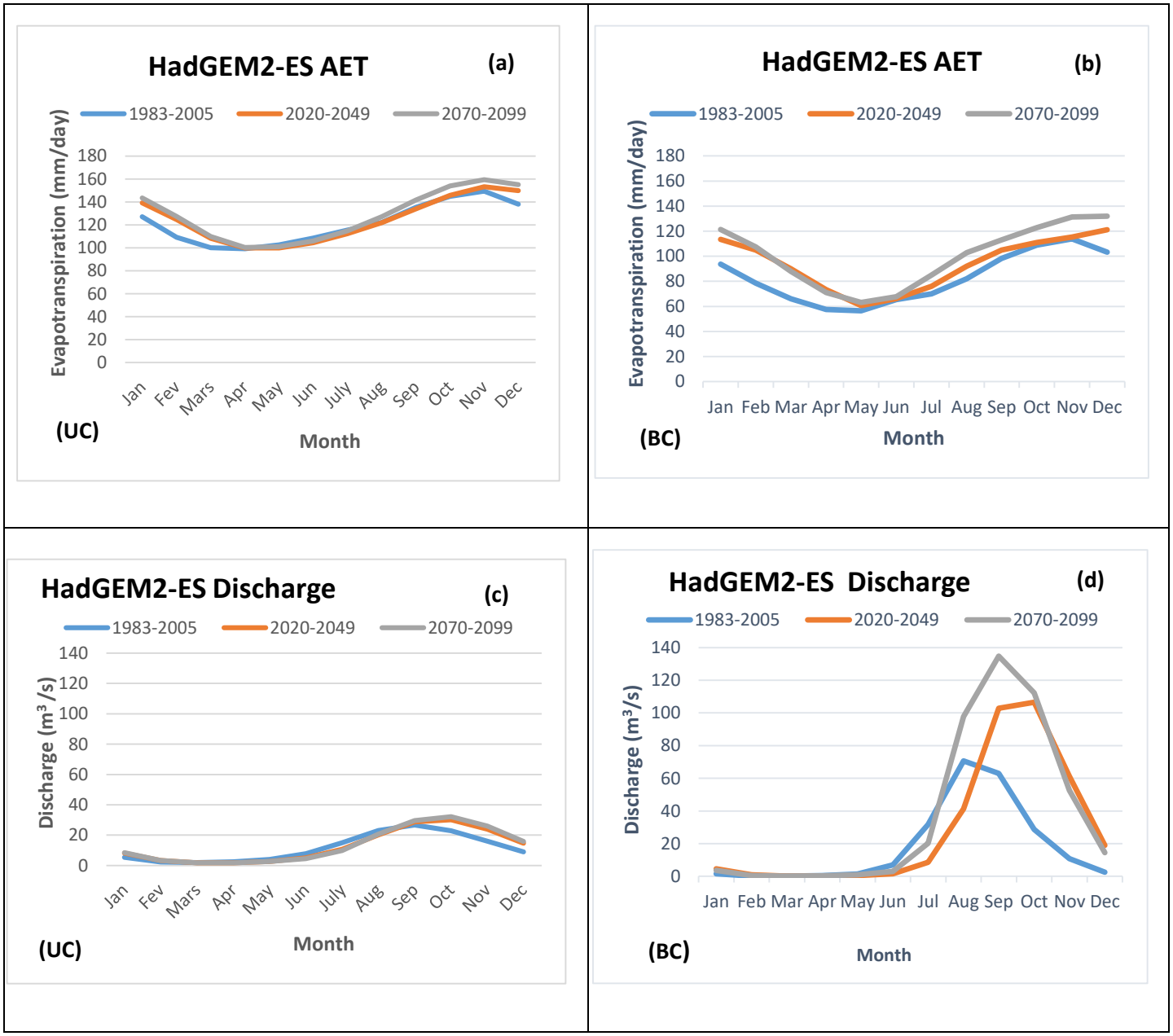

Figure 22. Climate change signal of Evapotranspiration and Discharge between the reference (1983-2005) and future (2020-2049 and 2070-2099) periods under RCP 4.5. (a) and (c)- uncorrected; (b) and (d)- bias corrected.

Overall, HadGEM2-ES model simulations reveal that precipitation, temperature, evapotranspiration and discharge will increase in future (2020-2049; 2070-2099) compared to the baseline (1983-2005). Bias correction application (quantile mapping) to the model output didn't alter the trend in climate change signal even though bias corrected values are higher than

uncorrected values for precipitation, temperature and discharge while lower for actual evapotranspiration.

Futhermore, HadGEM2-ES model simulations depict well the climate trend in Mono basin where during rainy season, there is an increase in discharge from August to October with one peak in September and another one in October (section 5.2. Discharge analysis).

GFDL-ESM2M model simulation (Figure 23-a, b, c d and Figure 24-a, b) projects an increase in future (2020-2049; 2070-2099) climate variables (precipitation, temperature and evapotranspiration) compared to the historical period (1983-2005). As HadGEM2-ES model simulations, both uncorrected and bias corrected climate variables simulated by GFDL-ESM2M present the same trend in climate change signal even though bias corrected precipitation, temperature and evapotranspiration are higher than those of uncorrected.

As presented in table 7, for uncorrected precipitation, precipitation change signal is up to 5% for the first future period (2020-2049), 9% for the second future period (2070-2099) compared to the reference period, whereas bias corrected precipitation shows that the change is respectively about 15% and 30%.

Table 7. Projected change of climate variables between the reference (1983-2005) and future (2020-2049; 2070-2099) with bias corrected and bias uncorrected GFDL-ESM2M simulations

GFDL-ESM2M	**Uncorrected**			**Bias corrected**		
Period	Historical (1983-2005)	Change (2020-2049)	Change (2070-2099)	Historical (1983-2005)	Change (2020-2049)	Change (2070-2099)
Precipitation (mm)	1398	+5%	+9%	1228	+15%	+30%
Temperature (°C)	24.72°C	0.95°C	+1.65°C	24.72	+6.50°C	+7.41°C
AET (mm)	557	+138%	+155%	1047	+29%	+44%
Discharge (mm/day)	834	-82%	-86%	196	-58%	-44%

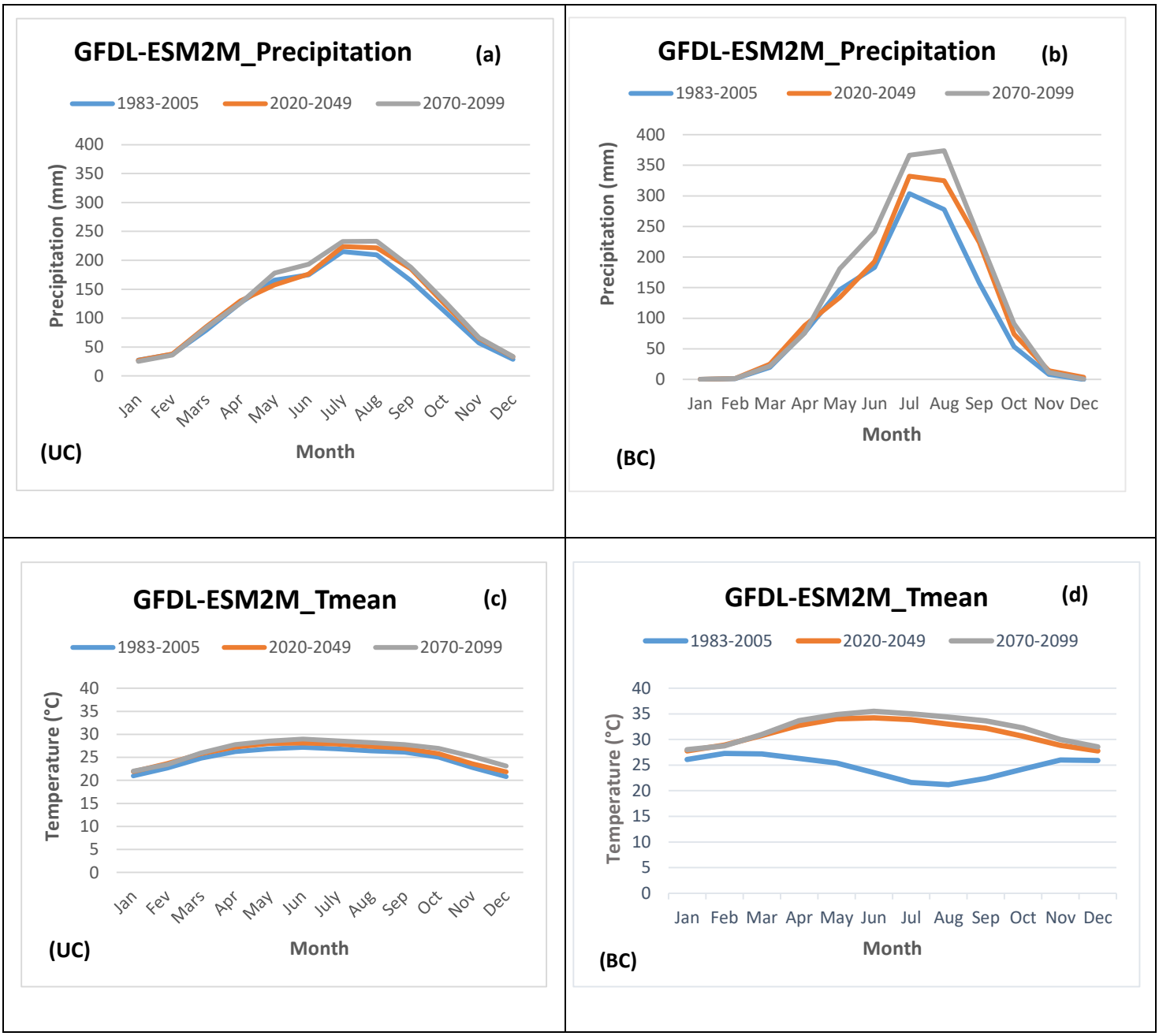

Figure 23. Climate change signal of precipitation and Temperature (Tmean), between the reference (1983-2005) and future (2020-2049 and 2070-2099) periods under emission scenario RCP 4.5.RCP 4.5. BC is bias corrected and UC refers to uncorrected bias (GFDL- ESM2M); (a) and (c)- uncorrected; (b) and (d)- bias corrected.

Uncorrected temperature varies from 0 to 0.95°C (2020-2049) then from 0.95 to 1.65°C (2070-2099) whereas bias corrected temperature ranges from 0 to 6.5° (2020-2049) , then from 6.50° to 7.41°C (2070-2099), (Table 7). This means, quantile mapping bias correction did not change the climate trend simulated by GFDL-ESM2M. Besides, the model depict the rainfall trend within Mono basin (Figure 23b), the main rainy season from J une to October with the monthly maximum rainfall observed in september.

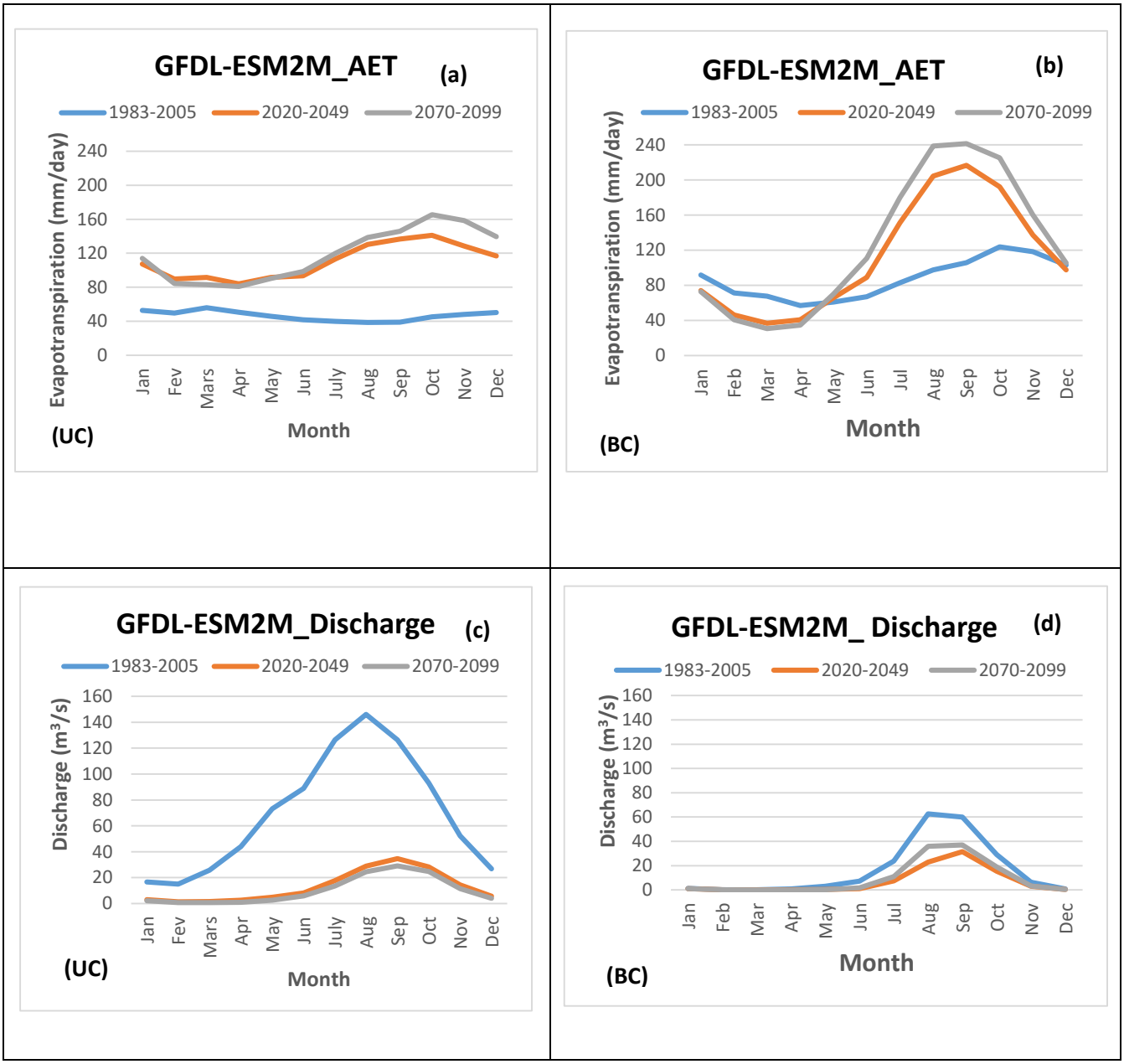

Figure 24. Climate change signal of evapotranspiration and discharge between the reference (1983-2005) and future (2020-2049 and 2070-2099) periods under RCP 4.5 (GFDL-ESM2M); (a) and (c)- uncorrected; (b) and (d)- bias corrected.

For the GFDL-ESM2M simulation under RCP 4.5, Figure 24 (c, d) illustrates that historical discharge are higher than future discharge. Bias corrected discharges are lower than uncorrected one. According to the change in the signal (Table 7), compared to the historical period, there will be a decrease in discharge about 58% by 2050 and 44% by 2100 for bias corrected while 82% and 86% for bias uncorrected. The decrease in future discharge could be due to the increase in future evapotranspiration which ranges between 29% and 44% with precipitation which varies between 15% and 30% as well as temperature from 6.50° to 7.41°C. Those values are higher than those of HadGEM2-ES model which are about 9% and 20% (Evapotranspiration), 19% and 35% (Precipitation), 1.17°C and 3.20°C (temperature) and 59% and 102% (Dsicharge) respectively by 2050 and 2100.

5.5. Flood frequency analysis and evaluation of its change due to climate effects

This section presents the results obtained from. Flood frequency analysis using Hyfran software verion 1.1. to analyse the relationships between flood quantile and its frequency of occurrence. A number of probability distributions were used and the corresponding BIC and AIC were computed and presented in Table 8 and table 9.

5.5.1. Determination of best-fit probability distribution

Table 8 and Table 9 show the distributions used and the corresponding performance criteria for the two models. It can be noticed that for the historical period of 1983- 2005, and future periods (2020-2049; 2070-2099), Weibull distribution presents the lower BIC and AIC compared to the Generalized Extreme value (GEV), Gumbel and Pearson type III using both Maximum Likelihood and Method of moments. As shown by the graph in Figure 25. Weibull distribution line (red) account for most of observation points. The probability distribution which has the lower BIC and AIC is the one fitting better the data series (section 2.3.4). Hence, Weibull fitting the best the discharge series for both HadGEM2-ES and GFDL-ESM2M models / HBV outputs.

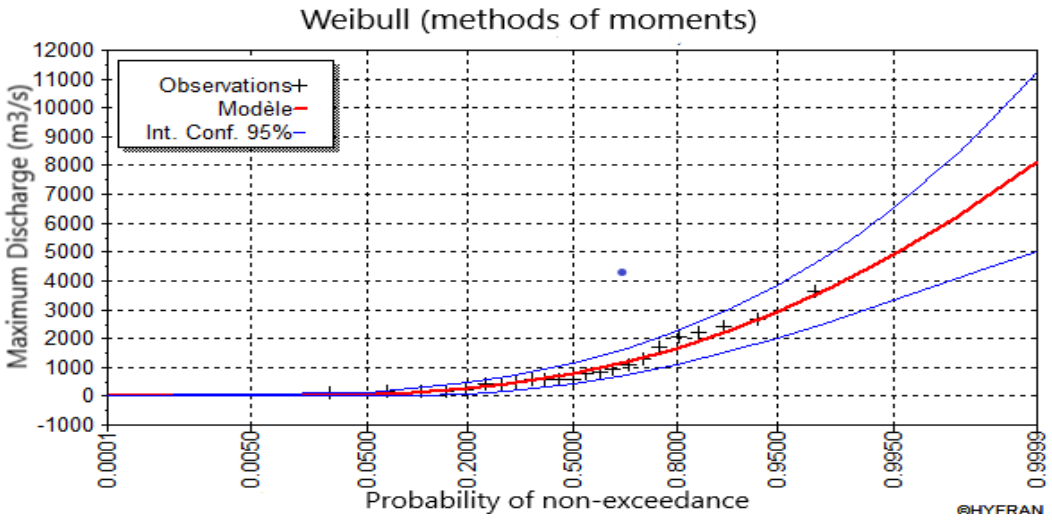

Figure 25.Weibull distribution

Table 8. Comparison of the criteria values for different probability distributions for HadGEM2-ES. BIC: Bayesian Information criterion, AIC: Akaike Information Criterion and XT: Quantile

HadGEM2-ES										
Probability Distribution	Parameter Estimation method	Period 1983-2005			Period 2020-2049			Period 2070-2099		
		XT	BIC	AIC	XT	BIC	AIC	XT	BIC	AIC
Weibull	Maximum Likelihood	4089	371.3	369.05	5618	506.70	503.9	5374	511.358	508.56
Generalized Extreme value, GEV		11228	374.6	371.192	5210	511.676	508.9	5945	512.542	509.74
Gumbel (GEV I)		3533	377.44	375.164	9740	511.75	507.5	6124	515.858	511.65
Weibull	Method of moments	4339	371.47	369.197	5852	506.81	504	5515	511.426	508.62
Generalized Extreme value, GEV		4033	378.71	376.44	5672	512.49	509	5887	512.497	509.7
Pearson type III		4107	379.76	376.353	5698	513.98	509.8	5507	516.448	512.24
Gumbel (GEV I)		4117	381.19	377.786	5723	515.60	511.4	5532	516.517	512.31

Table 9. Comparison of the criteria values for different probability distribution, (GFDL-ESM2M)

GFDL-ESM2M										
Probability Distribution	Parameter Estimation method	Period 1983-2005			Period 2020-2049			Period 2070-2099		
		XT	BIC	AIC	XT	BIC	AIC	XT	BIC	AIC
Weibull	Maximum Likelihood	2278	353	351	1442	422	420	1461	430	428
Generalized Extreme value, GEV		2518	354	352	6563	425	421	1528	434	431
Gumbel (GEV I)		2631	357	353	1302	430	427	1667	437	433
Weibull	Method of moments	2350	353	351	1491	423	420	1469	430	428
Generalized Extreme value, GEV		2513	354	352	1422	430	428	1504	434	431
Pearson type III		2393	357	353	1369	434	430	1376	438	434
Gumbel (GEV I)		2407	357	354	1380	435	431	1374	439	435

5.5.2. Climate change impact on flood frequency

Understanding the climate change impact on the hydrologic cycle evolution is one of the major challenges for water resources management. Recent climate changes have had serious impacts on the magnitude and frequency of floods in many regions of the world (IPCC, 2014). This section therefore, presents the results and analysis about the impact of climate change on flood frequency in the study area, Mono Lower Basin. Table 10 presents the probability of non-exceedance (q), the flood quantile (XT) as well as the corresponding return period (T), for the historical (1983-2005) and future periods (2020-2049; 2070-2099). Those results were obtained from Weibul distribution (method of moments) with Hyfran software.

Table 10. Frequency analysis results for the periods 1983-2005, 2020-2049 and 2070-2099, Weibull distribution (Method of moments), HadGEM2-ES and GFDL-ESM2M

Models		**HadGEM2-ES**			**GFDL-ESM2M**		
T	q	XT (1983- 2005)	XT (2020-2049)	XT (2070-2099)	XT (1983- 2005)	XT (2020-2049)	XT (2070-2099)
50	0.98	3740	5140	5040	2150	1300	1320
20	0.95	2940	4160	4340	1860	1040	1110
10	0.90	2320	3370	3750	1610	836	931
5	0.80	1680	2530	3080	1320	619	735
3	0.6667	1190	1870	2490	1070	450	572
2	0.50	782	1300	1930	830	306	422

To reduce the uncertainties in climate model simulations, Hydrological model HBV, Eto calculator, quantile mapping method, Hyfran software, the analysis was concentrated on change in quantiles which is common in scenario analysis (Hounkpè et al., 2018) rather than absolute values. The change in flood frequency over the future periods (2020-2049; 2070-2079) is presented in Table 11. HadGEM2-ES reveals an increase in future quantile change whereas GFDL-ESM2M shows a decrease in future quantiles compared to the historical quantiles. For HadGEM2-ES the change ranges between 34.79% and 66.24% for the period (2020-2049 and 26.95% to 146.80% for 2070-2099. As for, GFDL-ESM2M, it varies from -63.13% to -36.59% for 2020-2049 and from -49.15% to -37.44% for 2070-2099. Therefore, while HadGEM2-ES indicated that flood frequency will increase in the middle and by the end of 21st century due to the climate change, GFDL-ESM2M presents a decreasing trend.

Table 11. Percentage change in future quantiles relative to the historical quantiles

	HadGEM2-ES		**GFDL-ESM2M**		**Average**	
T	2020-2040	2070-2099	2020-2049	2070-2099	2020-2040	2070-2099
50	+37.43	+34.75	-39.53	-38.60	-2.1	-3.85
20	+41.49	+47.61	-44.08	-40.32	-2.59	+7.29
10	+45.25	+61.63	-48.07	-42.17	-2.82	+19.46
5	+50.59	+83.33	-53.10	-44.31	-2.51	+39.02
3	+57.14	+109.24	-57.94	-46.54	-0.8	+62.7
2	+66.24	+146.80	-63.13	-49.15	+3.11	+97.65

As also shown by Table 11, for both future periods (2020-2049; 2070-2099), when the return period increases, the percentage changes decrease. In other words, higher return periods correspond to lower variation. Furthermore, according to HadGEM2-ES model, change in quantiles for the period 2070- 2099 are higher than those of 2020-2049 for the return periods 20, 10, 5, 3 and 2 while lower for GFDL-ESM2M model . On one hand, higher discharge will be recorded by 2100 compared to 2050 as well as the historical period (1983-2005) based on HadGEM2-ES projection. On another hand, lower discharge will be observed in future period compared to the past based on GFDL-ESM2M projection. The average change resulting from the two models indicated a decrease for the return periods 50, 20, 10, 5, 3 and 50 respectively for future periods 2020-2049 and 2070-2099 whereas an increase for the return periods 3, 2 (2020-2049) and 20, 10, 10, 5, 3 and 2 (2070-2099).

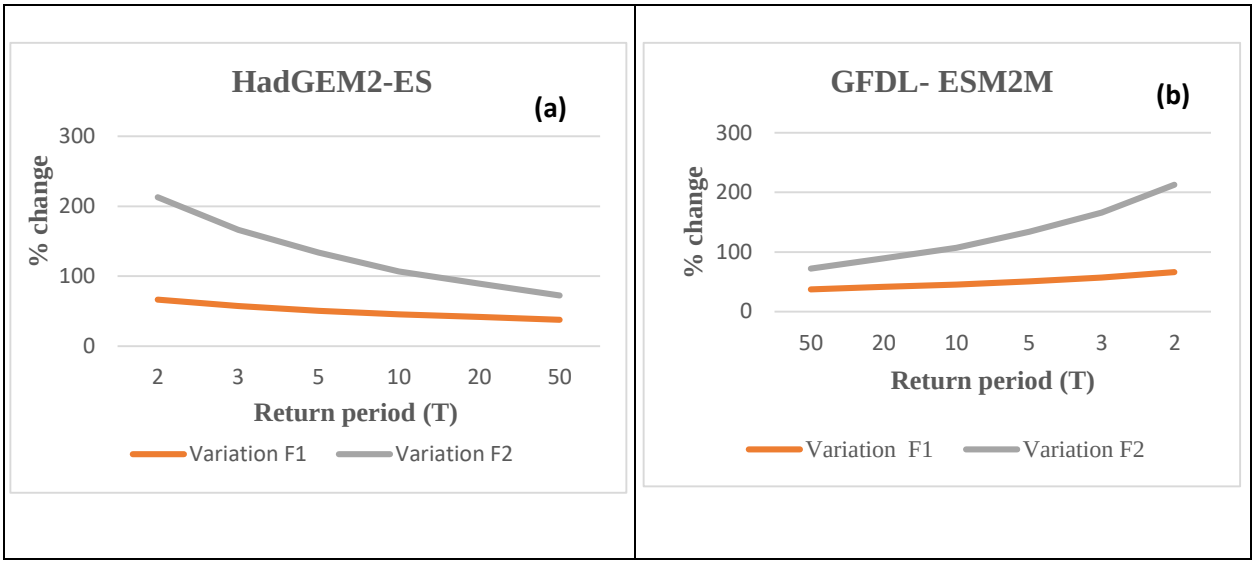

Figure 26. Change in future quantiles based on historical quantiles

CHAPTER SIX

6. CONCLUSION AND RECOMMENDATIONS

The main objective of this research study achieved through three specific objectives. Firstly, HBV-light model (Hydrologiska Byråns Vattenbalansavdelning) version 4.0.0.22 was calibrated over the period 1986- 1990 and validated on 1991- 1992, and in years 1985 and 2010. Satisfactory results were obtained during the calibration and validation periods except the independent years 1985 and 2010 where the simulated hydrograph are quite underestimated compared to the observed one.

Secondly, two WASCAL regional climate models (HadGEM2-ES and GFDL-ESM2M) under the Representative Concentration Pathway (RCP 4.5), were used as input to HBV-light model to evaluate the climate change signal on water balance components (precipitation, temperature, evapotranspiration and discharge) in the Lower part of Mono basin. The ability of the climate models to simulate historical climate and discharge was evaluated prior to future climate change impact assessment.This showed that bias correction was important for the models output in order to accurately reproduce observed data. Bias correction method applied in this research, quantile mapping, proved not to alter projected water balance components change signal. This result indicates the same trend in climate variables for both models with and without bias correction. The models exhibits an overall increase in future precipitation and temperature. HadGEM2-ES and GFDL-ESM2M project respectively an increase of about 19% and 15% for precipitation; 0 to 1.17°C and 0 to 6.5°C for temperature by 2050 while 35% and 30% for precipitation; 0 to 7.41°C for temperature by 2100. Given these characteristics of the climate, the discharge of Mono River at Athiémé will undergo some modifications. HadGEM2-ES model illustrates an increase in discharge signal change about 59% by 2050 and 102% by 2100 whereas GFDL-ESM2M simulations reveals a decrease in future discharge about 58% by 2050 and 44% by 2100.The opposite signals in discharge based on different climate products make it difficult to consider the results for decision making. More climate products, CORDEX Africa data and Ensembles could be considered for future research in Mono catchment.

Thirdly, climate change impact on flood frequency was assessed in the study area. The finding underline While HadGEM2-ES simulations under RCP 4.5 exhibits an increase in flood frequency,

GFDL-ESM2M shows a decrease. The average change of HadGEM2-ES and GFDL-ESM2M models project a decrease for the return period 50 and an increase for the return period 3 and 2.

The applied Hydrological model, HBV-light version 4.0.0.22 proved to simulate discharge in Mono Basin. The adopted " quantile mapping", approach also appears suitable for minimizing bias in climate models output without altering the trend in climate change signal.

The results further highlight on one hand, the need for a larger ensemble of projections to better assessing the impacts of climate change on water balance components and flood frequency in the Mono Basin .On another hand, land use could be considered as it is also an issue to improve the findings in further studies especially for designing water management interventions or strategies in term of practical relevance. Two models are not enough to conclude on the trend and climate change signal in the study area. In addition, the use of several hydrological models could help to properly evaluate the results.

Therefore, assessing future climate change impact on water balance components and flood frequency in the Basin needs to be updated with the improvement of climate projections. It is also necessary on one hand, to pursue and strengthen existing flood management strategies in areas located in the Lower part of Mono Basin and on another hand to develop adaptation and contingency plans for the whole Mono river Basin.

REFERENCES

Adegoke, B. Y. J., Sylla, M. B., Taylor, C., & Klein, C. (2019). Chapter 1 : On the 2017 Rainy Season Intensity and Subsequent Flood Events Over West Africa. https://doi.org/10.33183/rccs.2019.p10

Ago, E. E., Petit, F., & Ozer, P. (2005). Analysis of flood downstream from the Nangbeto dam on the Mono River (Togo and Benin), 1–14.

Alib, M. F., Mane, N. F., Faiza, N., Rahrnanb, A., Pahang, U., Alam, U. S., & Razak, J. T. (2016). Rainfall Data Analysis in Langat River Basin Using Hyfran. Journal of Engineering and Applied Sciences, 11(11), 2360–2365.

Amoussou, E. (2010). Variabilité pluviométrique et dynamique hydro-sédimentaire du bassin versant du complexe fluvio-lagunaire Mono- Ahémé-Couffo (Afrique de l'ouest).

Amoussou, E. (2015). Analyse hydrométéorologique des crues dans le bassin-versant du Mono en Afrique de l'Ouest avec un modèle conceptuel pluie- débit. Fondation Maison Des Sciences de l'homme, FMSH-WP-20, 1–27. Retrieved from http://www.fmsh.fr

Asumadu-Sarkodie, S., & Owusu, P. A. (2016). A review of Ghana's energy sector national energy statistics and policy framework. https://doi.org/10.1080/23311916.2016.1155274

Bates, B., Kundzewicz, S., & Palutikof, J. (2008). Climate Change and Water Technical Paper of the Intergovernmental Panel on Climate Change.

Bergström. (1992). The hbv model - its structure and applications.

Booij, M. J. (2005). Impact of climate change on river flooding assessed with different spatial model resolutions, 303, 176–198. https://doi.org/10.1016/j.jhydrol.2004.07.013

Brocca, L., Melone, F., & Moramarco, T. (2011). Soil moisture estimation through ASCAT and AMSR-E sensors: An intercomparison and validation study across Europe. Hydrological Processes, 3390–3408.

Cayan, D., Maurer, E., Dettinger, M., Tyree, M., & Hayhoe, K. (2008). Climate change scenarios for the California region. Climate Change, 21–42.

Christensen, J., Boberg, F., & Lucas-Picher, P. (2008). On the need for bias correction of regional climate change projections of temperature and precipitation. Retrieved from https://doi.org/10.1029/2008GL035694

Claps, P., & Laio, F. (2003). Can continuous streamflow data support flood frequency analysis? An alternative to the partial duration series approach. Water Resources. Retrieved from doi:10.1029/2002WR001868

Ehsanzadeh, E., El Adlouni, S., & Bobée, B. (2010). Frequency analysis incorporating a Decision Support System (DSS) for hydro-climatic variables. Journal of Hydrologic Engineering, 15:11, 861–881.

FAO, Leuven, U., & RAES, D. (2012). Eto calculator version 3.2, Land and Water Digital Media Series N°36. Retrieved from http://www.fao.org/nr/water/ETo.html

Fernando. (2014). Inondations dans la basse vallée du Mono typologie et manifestations.

Flemming, K., Tregoning, P., Kuhn, M., Purcell, A., & McQueen, H. (2012). The effect of melting land-based ice masses on sea-level around the Australian coastline. Australian Journal Earth of Sciences, 59(4), 457–467.

Gaba, O., Biao, I., Alamou, A., & Afouda, A. (2015). An Ensemble Approach Modelling to Assess Water Resources in the Mékrou Basin, Benin. Science Publishing Group, 22–32.

Gayathri. (2015). A Review on Hydrological Models ENGINEERING (ICWRCOE 2015), (July). https://doi.org/10.1016/j.aqpro.2015.02.126

Ghorbani, M. A., Ruskeep, H., Singh, V. P., & Sivakumar, B. (2010). Flood frequency analysis using Mathematica, 34, 171–188. https://doi.org/10.3906/muh-1002-2

Giuliano, D., Laio, F., & Montanari, A. (2009). Design flood estimation using model selection criteria. Physics and Chemistry of the Earth, 34(10–12), 606–611. https://doi.org/10.1016/j.pce.2008.10.066

Grillakis, M. G., Koutroulis, A. G., Daliakopoulos, I. N., & Tsanis, I. K. (2017). A method to preserve trends in quantile mapping bias correction of climate modeled temperature. Earth System Dynamics, 889–900.

Grillakis, M. G., Tsanis, I. K., & Koutroulis, A. G. (2010). Application of the HBV hydrological model in a flash flood case in Slovenia. Natural Hazards and Earth System Sciences Application, 2713–2725. https://doi.org/10.5194/nhess-10-2713-2010

Grillakis, M., Koutroulis, A., & Tsanis, I. (2013). Multisegment statistical bais correction of daily GCM precipitation output. Geophysic, Journal Of, 118, 3150–3162. Retrieved from https://doi.org/10.1002/jgrd.50323, 2013.

Gudmundsson, L., Engen-skaugen, T., Bremmes, J., & Haugen, J. (2012). Hydrology and Earth System Sciences Technical Note : Downscaling RCM precipitation to the station scale using statistical transformations – a Technical Note : Downscaling RCM precipitation to the station scale using statistical transformations – a compari. Hydrology and Earth System Sciences, 3383–3390. https://doi.org/10.5194/hess-16-3383-2012

Guha-sapir, D. (2010). Guha-Sapir 2011.

Hagemann, S., Chen, C., Clark, D., Folwell, S., Gosling, S., Haddeland, I.,Wiltshine, A. (2013). Climate change impact on available water resources obtained using multiple global climate and hydrology models. Earth System Dynamics, 4, 129–144. Retrieved from https://doi.org/10.5194/esd-4-129-2013

Harding, R., Weedon, G., Lanen, V, H., & Clark, D. (2014). The future for global water assessment. Journal of Hydrology, 518, 186–193. Retrieved from https://doi.org/10.1016/j.jhydrol.2014.05.014,

Hargreaves, G., & Samani, Z. (1982). Estimating potential evapotranspiration. ASCE, 223–230.

Harlin, J. (1992). Modelling the hydrological response of extreme floods in Sweden. Hydrology, Nordic, 227–244.

Hayhoe, H. (2004). Emissions pathways, climate change, and impacts on California.

Heinzeller, D., Dieng, D., Smiatek, G., Olusegun, C., & Klein, C. (2018). The WASCAL high-resolution regional climate simulation ensemble for West Africa : concept , dissemination and assessment. Earth System Science Data, 815–835. Retrieved from https://doi.org/10.5194/essd-10-815-2018

Houngue, N. R. (2018). Assessment of mid-century climate change impacts on mono river's downstream inflows. faculty of art and humanities department of geography.

Hounkpè, J., Diekkrüger, B., Afouda, A. A., & Crepin, L. O. (2018). Land use change increases flood hazard: a multi-modelling approach to assess change in flood characteristics driven by socio-economic land use change scenarios. Journal of the International Society for the Prevention and

Mitigation of Natural Hazards, 68, 32. https://doi.org/10.1007/s11069-018-3557-8

Icyimpaye, G. (2018). Implementation of hydrological and hydraulic models to forecast river flood risks and proposition of management measures. Case study of Nyabugogo River basin in Rwanda Chair. Pan-african university institute for water and energy sciences (including climate change) master.

Ines, A., & Hansen, J. (2006). Bias correction of daily GCM rainfall for crop simulation studies, 138, 44–53. Retrieved from https://doi.org/10.1016/j.agrformet.2006.03.009

IPCC. (2012). Summary for Policymakers. In Managing the Risks of Extreme Events and Disasters to Advance Climate Change Adaptation. A special Report of Working Groups I and II of the Intergovernmental Panel on Climate Change.

IPCC. (2014). Climate Change 2014 Synthesis Report.

Khaliq, M., Ouarda, J., Ondo, P., Gachon, P., & Bobée, B. (2006). Frequency analysis of a sequence of dependent and/or non-stationary hydro-meteorological observations: a review. Hydrology, Journal Of, 329, 534–442.

Lamboni, B., Emmanuel, L. A., Manirakiza, C., & Djibib, Z. M. (2019). Variability of Future Rainfall over the Mono River Basin of West-Africa. American Journal of Climate Change, 8, 137–155. https://doi.org/10.4236/ajcc.2019.81008

Lindström, G., & Harlin, J. (1992). Spillway design floods in Sweden. II: Application and sensitivity analysis. Hydrological Sciences Journal, 521–539.

Maghsood, F. F., Reza, A., Bavani, M., Panahi, M., & Berndtsson, R. (2019). Climate Change Impact on Flood Frequency and Source Area in Northern Iran Climate Change Impact on Flood Frequency and Source Area in Northern Iran under CMIP5 Scenarios, (February), 23. https://doi.org/10.3390/w11020273

Manyifika, M. (2015). Diagnostic assessment on urban floods using satellite data and hydrologic models in Kigali, Rwanda.

Maurer, E., & Hidalgo, H. (2008). Utility of daily vs. monthly large scale climate data: An intercomparison of two statistical downscaling methods. Hydrology and Earth System Sciences, 551–563.

Miller, J., Immerzeel, W., & Rees, G. (2012). Climate change impacts on glacier hydrology and river discharge in the Hindu kush-Himalayas: a synthesis of the scientific basis, 461–467.

Millington, N., Das, S., & Simonovic, S. (2011). The Comparison of GEV, Log-Pearson Type 3 and Gumbel Distributions in the Upper Thames River Watershed under Global Climate Models, (September), 54.

Mizukami, N., Rakovec, O., Newman, A., Clark, M., Wood, A., Gupta, H., & Kumar, R. (2018). On the choice of calibration metrics for " high flow " estimation using hydrologic models. Hydrology and Earth System Sciences, (August), 1–16.

Mkilima, T. (2018). Modeling of storm water runoff for improving floods resilience, water supply, soil and ecological conservation. the case of msimbazi catchment in dar es salaam, tanzania. pan-african university institute for water and energy sciences (including climate change.

Mujumdar, P. P., & Kumar, D. N. (2012). More Information - Www.Cambridge.Org/9781107018761. https://doi.org/1753-2000-2-33 [pii]\n10.1186/1753-2000-2-33

Mureithi, I. N., Shrestha, B., & Kingma, C. (2015). Flash Flood Hazard and Coping Strategies in Urban

Areas : Case Study in Mpazi Catchment , Kigali, 1–8.

N'Tcha M'Po, Y., Lawin, A., Oyerinde, G., Yao, B., & Afouda, A. (2016). Comparison of daily precipitation bias correction methods based on four regional climate model outputs in Ouémé Basin, Benin. Hydrology, 4, 58–71.

Ntajal, J. (2016). Rainfall trends and flood frequency analyses in the lower-mono river in togo, west africa. international journal of advance research, ijoar .org, 4(october), 12.

Ntajal, J., Lamptey, B. L., & Mianikposogbedji, J. (2018). Flood Vulnerability Mapping in the Lower Mono River Basin in Togo, West Africa. International Journal of Scientific & Engineering Research, 7(October 2016), 12.

Ohl, C. A. (2000). Flooding and human health. Bmj, 321(7270), 1167–1168. https://doi.org/10.1136/bmj.321.7270.1167

Oyerinde, G. (2016). Climate change in the Niger basin on hydrological properties and functions of Kainji lake, West-Africa.PhD dissertation, Université d'Abomey-Calavi.

Pappenberger, F., Maltgen, P., & Beven, K. (2006). Influence of uncertain boundary conditions and model structure on flood inundation predictions. Advances in Water Resources, 1430–1449.

Pool, S., Eth-bereichs, E. D. W., Pool, S., Vis, M., & Seibert, J. (2018). Evaluating model performance : towards a non-parametric variant of the Kling-Gupta efficiency. Hydrological Sciences Journal, 0(0), 32. https://doi.org/10.1080/02626667.2018.1552002

Prudhomme, C., Wilby, R., Crooks, S., Kay, A., & Reynard, N. (2013). Climatevchange and river flooding: part 1 classifying the sensitivity of British catchments. Climate Change, 119, 933–948.

Radchenko, I. (2016). Impact of climate change on the contribution of second order tributaries to the water balance of the Ferghana Valley. Agricultural Sciences, Nutritional Sciences, and Environmental Management Justus-Liebig-University Giessen.

Ramesh. (2012). Floods in a changing climate Exytreme precipitation. Clinical Orthodontics and Research (Vol. 2). https://doi.org/10.1016/j.cub.2015.10.018

Rao, R., & Hamed, H. (2000). Flood frequency analysis. London: CRC Press.

Salaheddine, E. A., & Bobée, B. (2015). Professeur , Département de Mathématiques et de statistique , Université de Moncton Professeur Émérite Version of the 13 th of January 2015 Note : Documents listed in the references (page 61) and marked by * are available when installing the DEMO versio, (1), 1–71.

Schwarz, G. (1978). Estimating the dimension of a model, 6, 461–464.

Seibert, J. (1997). Estimation of Parameter Uncertainty in the HBV Model, 28, 247–262.

Seibert, J. (2005). User ' s Manual, (November).

Sharma, D., Gupta, A., & Babel, M. (2007). Spatial disaggregation of bias-corrected GCM precipitation for improved hydrologic simulation:Ping River Basin, Thailand. Hydrology and Earth System Sciences.

Shrestha, S., & Lohpaisankrit, W. (2016). Flood hazard assessment under climate change scenarios in the Yang River Basin , Thailand. International Journal of Sustainable Built Environment, (October), 14. https://doi.org/10.1016/j.ijsbe.2016.09.006

Singh, V. (1996). Entropy-based parameter estimation in hydrology. Dordrecht: Kluwer Academic Publishers. Dordrecht: Kluwer Academic Publishers.

Teutschbein, C., & Seibert, J. (2012). correction of regional climate model simulations for hydrological climate-change impact studies: Review and evaluation of different methods. Journal of Hydrology, 456–457, 12–29.

Themeßl, M., Gobiet, A., & Leuprecht, A. (2011). Empirical-statistical downscaling and error correction of daily precipitation from regional climate models. International Journal of Climatogy, 31, 1530–1544. Retrieved from doi:10.1002/joc.2168, 2011.

Ufe, Z. (2015). floods : Q & A. https://doi.org/10.1109/MSR.2017.5

UNISDR. (2005). Hyogo Framework for Action 2005-2015: Building the Resilience of Nations and Communities to Disasters. In Extract from the final report of the World Conference on Disaster Reduction (pp. 1–25). https://doi.org/10.1017/CBO9781107415324.004

Walz, B. Y., & Sassen, V. (2019). Chapter 3 : The Need for a Regional Service to Monitor Flood Hazard Events in West Africa. https://doi.org/10.33183/rccs.2019.p20

Wood, A., Leung, L., Sridhar, V., & Lettenmaier, D. (2004). Hydrologic Implications of Dynamical and Statistical Approaches to Downscaling Climate Model Outputs, Climatic Change. Retrieved from doi:10.1023/B:CLIM.0000013685.99609.9e

World Bank. (2011). Inondation au Benin: Rapport d'evaluation des Besoins Post Catastrophe. Retrieved from www.gfdrr.org/sites/gfdrr.org/files/GFDRR_Benin_PDNA_2010.pdf, access on 01/12/2013

APPENDIXES

Appendix 1: Rainfall data processing

A. Rainfall raw data

			PLU	IOMETRI	JOURNA	IERE AN	EE 1983		EDITE	LE /	/	
					-------	--						
TATI	N: AFAG	AN			PAYS	:			LATI	UDE :	.	
UMER	: 47	7			REGIO	:			LONG	TUDE:	.	
OTAL	PLUVIO.	564.0	m						ALTI	UDE :	M	
----	-------	-------	-------	-------	-------	-------	-------	-------	-------	-------	-------	-------
JOUR	JAN	FEV	MARS	AVR	MAI	JUIN	JLT	AOUT	SEPT	OCT	NOV	DEC
----	-------	-------	-------	-------	-------	-------	-------	-------	-------	-------	-------	-------
1	.	.	.	.	.	.	.	.	.	.	.	16.7
2	.	.	.	.	.	.	.	.	.	.	.	18.5
3	.	.	.	23.6	.	.	.	.	.	.	.	.
4	.	.	.	.	.	.	.	.	.	7.3	.	.
5	.	.	.	.	.	.	.	.	.	.	8.3	.
6	.	.	.	.	.	.	.	88.0	.	.	.	.
7	.	.	.	.	.	8.0	.	.	.	.	.	.
8	.	.	.	.	.	.	.	.	.	.	.	.
9	.	.	.	.	32.0	.	.	.	.	.	.	.
10	.	.	.	26.6	.	18.0	.	.	.	.	.	.

B. Rainfall data arranged using microsoft office excel

YEAR	DAY	JAN	FEV	MARS	APR	MAY	JUN	JUL	AUG	SEPT	NOV	OCT	DEC
1983	1	-99	-99	-99	-99	-99	-99	-99	-99	-99	-99	-99	16.7
1983	2	-99	-99	-99	-99	-99	-99	-99	-99	-99	-99	-99	18.5
1983	3	-99	-99	-99	23.6	-99	-99	-99	-99	-99	-99	-99	-99
1983	4	-99	-99	-99	-99	-99	-99	-99	-99	-99	7.3	-99	-99
1983	5	-99	-99	-99	-99	-99	-99	-99	-99	-99	-99	8.3	-99
1983	6	-99	-99	-99	-99	-99	-99	-99	88.0	-99	-99	-99	-99
1983	7	-99	-99	-99	-99	-99	8.0	-99	-99	-99	-99	-99	-99
1983	8	-99	-99	-99	-99	-99	-99	-99	-99	-99	-99	-99	-99
1983	9	-99	-99	-99	-99	32.0	-99	-99	-99	-99	-99	-99	-99
1983	10	-99	-99	-99	26.6	-99	18.0	-99	-99	-99	-99	-99	-99

C. Rainfall data transformed using R software

YEAR	DATA
1/1/1983	-99
1/2/1983	-99
1/3/1983	-99
1/4/1983	-99
1/5/1983	-99
1/6/1983	-99
1/7/1983	-99
1/8/1983	-99
1/9/1983	-99
1/10/1983	-99

D. Stations rainfall data combined in one table

YEARS	GRAND_POPO	ATHIEME	DOGBO	LOKOSSA	PJLONKLY	TCHETTI	SOKODE
1/1/1983	0	NA	0	0	0	0	-99
1/2/1983	0	NA	0	0	0	0	-99
1/3/1983	0	NA	0	0	0	0	-99
1/4/1983	0	NA	0	0	0	0	-99
1/5/1983	0	NA	0	0	0	0	-99
1/6/1983	0	NA	0	0	0	0	-99
1/7/1983	0	NA	0	0	0	0	-99
1/8/1983	0	NA	0	0	0	0	-99
1/9/1983	0	NA	0	0	0	0	-99
1/10/1983	0	NA	0	0	0	0	-99

E. Weighted coefficient, Thiessen polygon method

Station	Area	Weighted
Tabligbo	654.8660278	0.0283254
Dogbo-Tota	646.9470215	0.0279829
Tchetti	518.8549805	0.0224424
anie-mono	4292.790039	0.185679
Sotouboua	5413.100098	0.234137
Kpewa-Aledjo	353.7820129	0.0300552
Wahala	1371.280029	0.059313
Lonkly	1458.650024	0.063092
Athieme	87.2863007	0.0037755
Afagnan	31.3693008	0.0013568
Lokossa	201.1089935	0.0086987
Nangbeto	1438.849976	0.0622356
Atakpame	1583.550049	0.0684944
Amou-Oblo	1196.790039	0.0517656
Tchamba	1302.729981	0.0563479
Sokode	1670.319946	0.0849731
Penesoulou	341.0750122	0
Malfacassa	261.8389893	0.0113255
Bassila	294.2090149	0
Total	23119.39783	1

F. Thiessen polygon obtained using Arc GIS

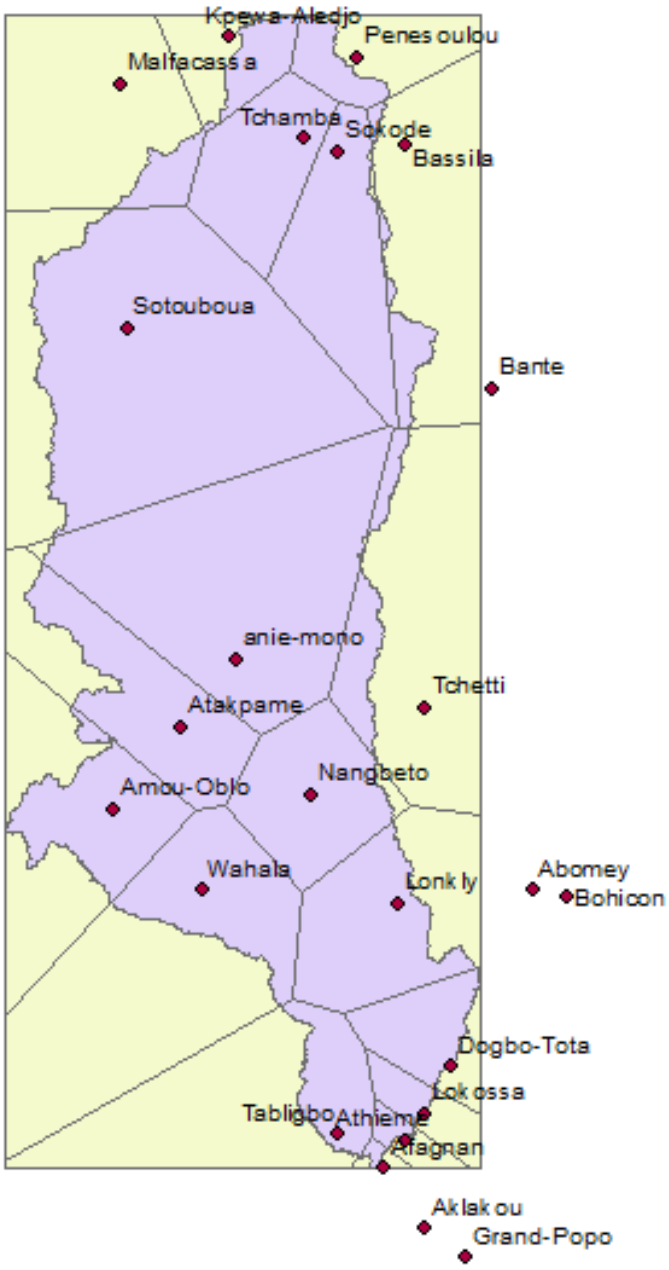

d

G. Discharge missing data from 1983 to 2010

YEAR	Missing data (%)	YEAR	Missing data (%)
1983	47.95	1997	1.92
1984	22.13	1998	0.27
1985	9.86	1999	67.76
1986	42.19	2000	19.40
1987	53.42	2001	100.00
1988	0.00	2002	51.23
1989	0.00	2003	67.95
1990	0.27	2004	49.18
1991	19.45	2005	76.71
1992	2.46	2006	66.58
1993	39.73	2007	51.51
1994	66.30	2008	82.24
1995	100.00	2009	0.00
1996	26.23	2010	0.00

G. Hydro-climatic stations coordinates

Stations	Longitude	Latitude
Afagnan	1.6167	6.5
Aklakou	1.7167	6.35
Athieme	1.6667517	6.566721
Dogbo-Tota	1.7833	6.75
Grand-Popo	1.8167001	6.2833
Lokossa	1.7167	6.6333
Tabligbo	1.5	6.5833
Sotouboua	0.9833	8.5667
Amou-Oblo	0.95	7.3833
anie-mono	1.25	7.75

Stations	Longitude	Latitude
Bohicon	2.06658117	7.1667474
Lonkly	1.650012	7.150017
Nangbeto	1.435876	7.420386
Tchetti	1.716667	7.63333
Wahala	1.1667	7.1833
Atakpame	1.1167	7.5833
Tchamba	1.416667	9.0333
Kpewa-Aledjo	1.2333	9.2833
Malfacassa	0.9667	9.1667
Sokode	1.5	9

e

Appendix 2: HBV model simulation for GFDLESM and HAGEM2 (RCP 4.5)

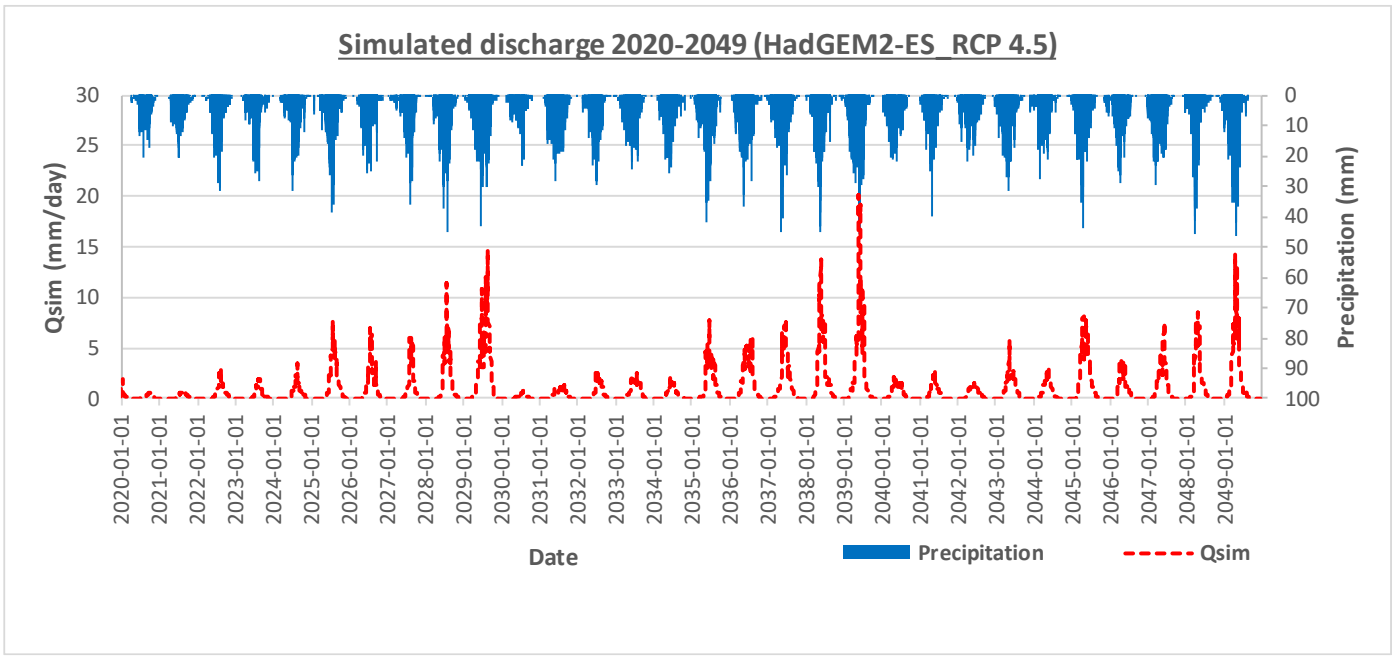

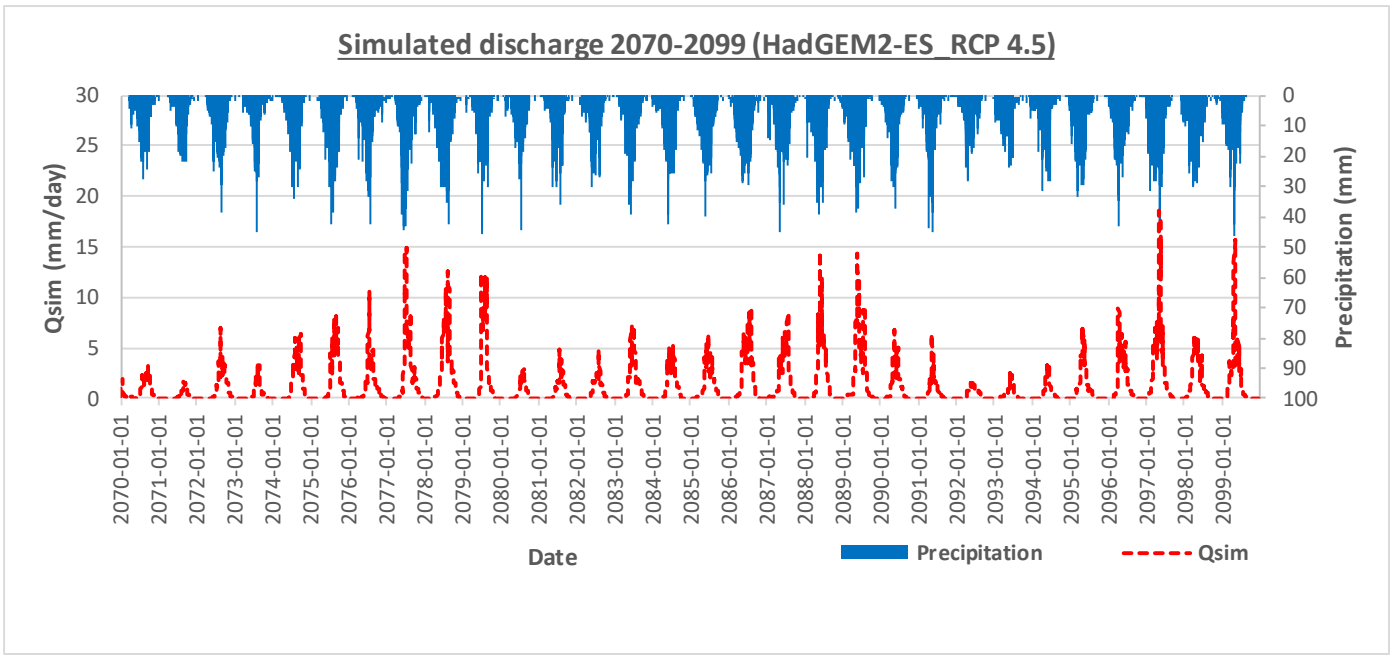

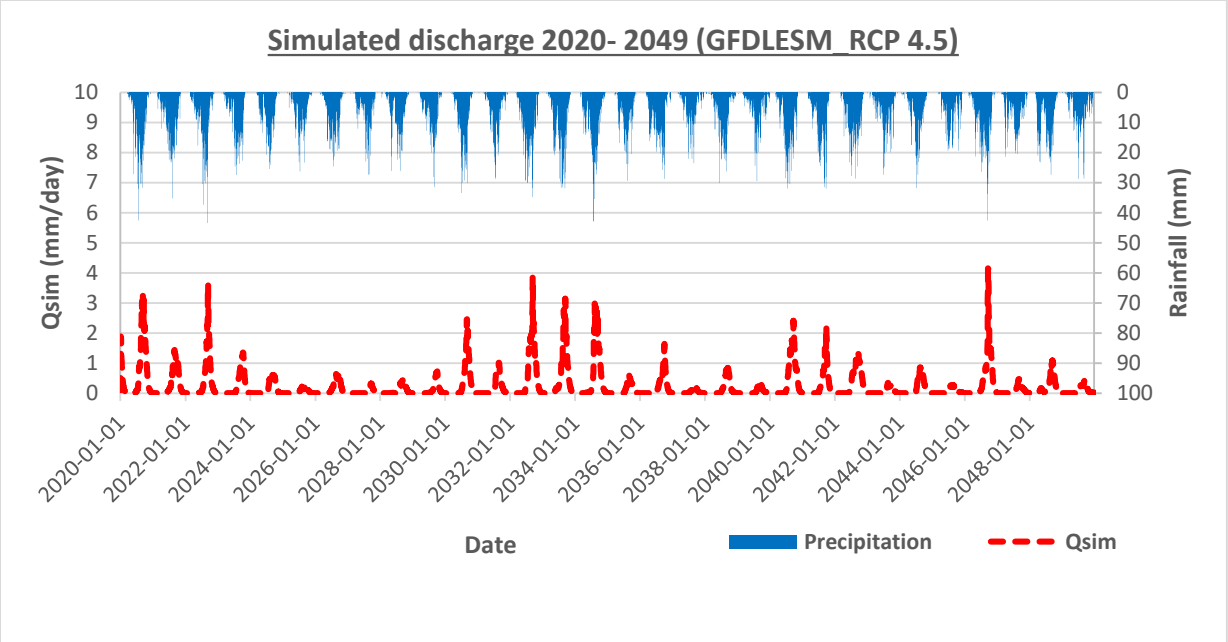
Simulated discharge 2020- 2049 (GFDLESM_RCP 4.5)
Qsim (mm/day)
Rainfall (mm)
Date
Precipitation
Qsim

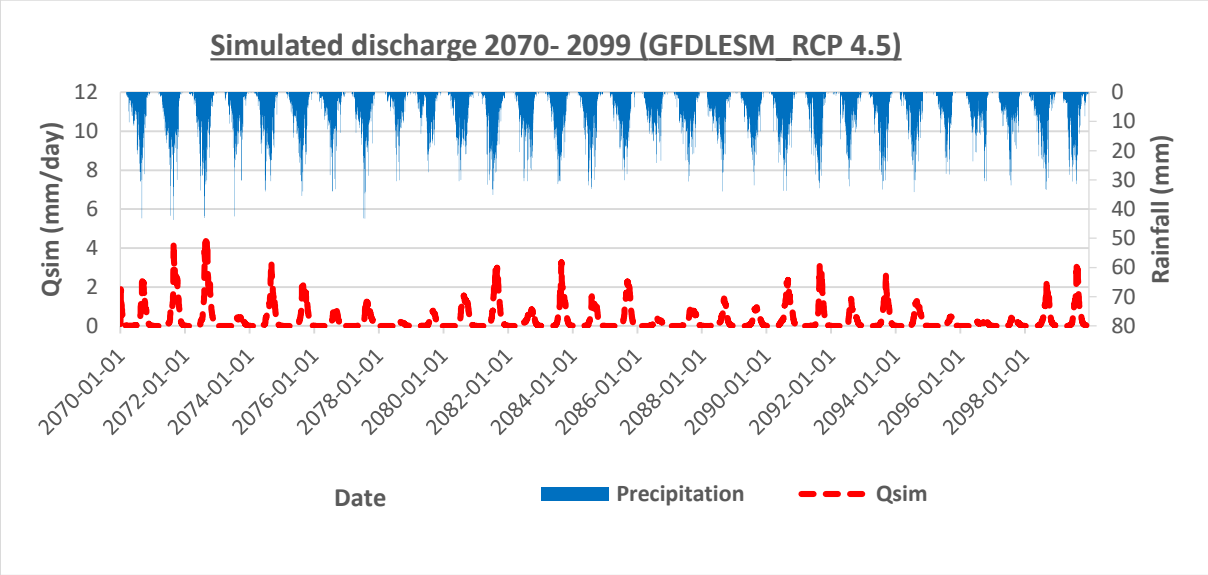
Simulated discharge 2070- 2099 (GFDLESM_RCP 4.5)
Qsim (mm/day)
Rainfall (mm)
Date
Precipitation
Qsim

g

Appendix 3: Climate Change Trend in Mono Basin